Electrochemical Nanomoulding Through Proteins

Daniel B. Allred

A dissertation submitted in partial fulfillment
of the requirements for the degree of

Doctor of Philosophy

University of Washington

2006

Program Authorized to Offer Degree:
Department of Chemical Engineering

INFORMATION TO USERS

The quality of this reproduction is dependent upon the quality of the copy submitted. Broken or indistinct print, colored or poor quality illustrations and photographs, print bleed-through, substandard margins, and improper alignment can adversely affect reproduction.

In the unlikely event that the author did not send a complete manuscript and there are missing pages, these will be noted. Also, if unauthorized copyright material had to be removed, a note will indicate the deletion.

ProQuest Information and Learning Company
300 North Zeeb Road
P.O. Box 1346
Ann Arbor, MI 48106-1346

University of Washington
Graduate School

This is to certify that I have examined this copy of a doctoral dissertation by

Daniel B. Allred

and have found that it is complete and satisfactory in all respects,
and that any and all revisions required by the final examining
committee have been made.

Chairs of the Supervisory Committee:

Daniel T. Schwartz

François Baneyx

Mehmet Sarikaya

Reading Committee:

Daniel T. Schwartz

François Baneyx

Mehmet Sarikaya

Date: 6/6/6

In presenting this thesis in partial fulfillment of the requirements for the doctoral degree at the University of Washington, I agree that the Library shall make its copies freely available for inspection. I further agree that extensive copying is allowable only for scholarly purposes, constistent with "fair use" as prescribed in the U.S. Copyright Law. Requests for copying or reproduction of this dissertation may be referred to Proquest Information and Learning, 300 North Zeeb Road, Ann Arbor, MI 48106-1346, 1-800-521-1600, to whom the author has granted "the right to reproduce and sell (a) copies of the manuscript in microform and/or (b) printed copies of the manuscript made from microform."

Signature 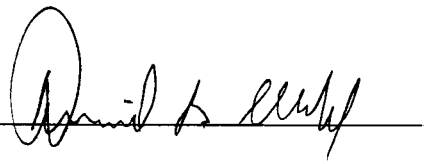

Date 6/6/16

University of Washington

Abstract

Electrochemical Nanomoulding Through Proteins

Daniel B. Allred

Chairs of the Supervisory Committee:
Professors Daniel T. Schwartz and François Baneyx
Department of Chemical Engineering
Professor Mehmet Sarikaya
Department of Materials Science and Engineering

The continued improvements in performance of modern electronic devices are directly related to the manufacturing of smaller, denser features on surfaces. Electrochemical fabrication has played a large role in continuing this trend due to its low cost and ease of scaleability toward ever smaller dimensions. This work introduces the concept of using proteins, essentially monodisperse complex polymers whose three-dimensional structures are fixed by their encoded amino acid sequences, as "moulds" around which nanostructures can be built by electrochemical fabrication.

Bacterial cell-surface layer proteins, or "S-layer" proteins, from two organisms – *Deinococcus radiodurans* and *Sporosarcina ureae* – were used as the "moulds" for electrochemical fabrication. The proteins are easily purified as micron-sized sheets of periodic molecular complexes with 18-nm hexagonal and 13-nm square unit cell lattices, respectively. Direct imaging by transmission electron microscopy on ultrathin noble metal films without sample preparation eliminates potential artifacts but still allows access to the high surface energy substrates necessary for high nucleation densities. Characterization involved imaging, electron diffraction, spectroscopy, and three-dimensional reconstruction. The S-layer protein of *D. radiodurans* was further subjected to an atomic force microscope based assay to determine the integrity of its structure and long-range order and was found to be useful for fabrication from around pH 3 to 12.

TABLE OF CONTENTS

LIST OF FIGURES

Figure Number Page

LIST OF TABLES

Table Number Page

ACKNOWLEDGMENTS

The author would like to thank the Army Research Office and the National Science Foundation in part for supporting this work under the DURINT and GEMSEC programs. Additional support also came from the Worldwide Universities Network under a Global Exchange Fellowship for a one-quarter stay in the United Kingdom to study electrochemical templating using a variety of self-assembled systems under Prof. Phil N. Bartlett. An Integrated Graduate Education Research Traineeship grant also provided additional support administered by the Center for Nanotechnology via the National Science Foundation.

Many thanks to Stuart Evans, Mamdouh Abdelsalem, and Mohamed Ghanem from the group in the University of Southampton. In the University of Washington, thanks are due to Hanson Fong, Thurston Herricks, Barry Lutz, Haixia Dai, Mirna Mujacic, Alvaro Presenda, Chris So, Tom Murray, and Melvin Zin. At Scripps Research Institute Anchi Cheng provided invaluable 3D reconstruction data. At the Pacific Northwest National Laboratory, thanks are owed to Don Baer, Mark Engelhardt, and Chongmin Wang. Finally, I would like to thank my advisors Daniel T. Schwartz, François Baneyx, and Mehmet Sarikaya, for their advice and guidance.

INTRODUCTION

The performance of many modern day products in industries ranging from food and drugs, cosmetics, textiles, and electronics, has benefited greatly from nanoscience and nanotechnology.[1] Nanoscience is an amalgam of physics, engineering, chemistry, statistical mechanics, and other disciplines that were integrated to describe unusual phenomena when observing systems at length scales larger than that of atoms and molecules but smaller than that of the wavelength of optical light. Nanotechnology refers to the suite of tools needed to create, visualize, manipulate, and characterize materials in this size spectrum.

Solution-borne nanomaterials display interesting properties, but the challenge is to arrange these nanomaterials on surfaces to permit communication to them with other components, such as electronic devices, thus permitting creating interesting functional devices. Popular ways to simulate the large scale fabrication attainable by using solution-based methods is to exploit self-assembling systems that can spontaneously order themselves on surfaces. Examples of such systems include anodized alumina [2] or phase-segregating emulsions.[3]

It has been suggested that crystalline proteins may make excellent alternative template systems.[4] Because biologically produced proteins are essentially perfect, *i.e.*, there is no polydispersity, the architecture of protein crystals are atomically well-defined. Thus, given a library of such proteins to choose from, one could select the protein that best suits one's fabrication needs, whether it is a given nanopore or nanoparticle size or separation or a series of parallel lines, and use it as a mask which will have nanoscale feature sizes and spacings with errors in the range of ångstroms.

It is then no surprise to find that many have already been using crystalline proteins for ordering materials at the nanoscale. The vast majority of prior methods have used

chemical precipitation methods to decorate the proteins with nanoparticles, either by reducing pre-complexed salts on them or by capturing preformed particles. Examples include cadmium sulfide nanoparticle formation on S-layer proteins from *Bacillus stearothermophilus*,[5] platinum nanoparticle formation on S-layer proteins from *S. ureae*,[6] organization of preformed gold nanoparticles on S-layer proteins from *D. radiodurans*,[7] and the organization of preformed gold and cadmium selenide-zinc sulfide nanoparticles on engineered chaperonin proteins from *Sulfolobus shibatae*.[8] The mentioned methods are ultimately solution-based methods and there is no means for contact to the surface except, perhaps to land the proteins on a surface and allow reflow, if the particles and proteins remain assembled during this process. Surface-directed fabrication approaches would be ideal over solution-based methods for this reason. A number of surface-oriented fabrication approaches have been explored previously. The most relevant approach is one where proteins on a surface are coated with metal from a vapor and are subsequently ion-milled to reveal the pattern.[9-13] Another approach uses an electron beam to locally reduce trapped metal salts in the cavities of the protein structure.[14]

A more general strategy would be useful for filling the fine structures between, and possibly within, the proteins' nanoscale architecture. Modern integrated circuit fabrication technology uses the method of electrochemical deposition as the process of choice for building up the various layers of metallic interconnects and this method is expected to continue to play a dominant role in future device fabrication.[15] It was surprising to find a dearth of previously published successful implementation of proteins as masks for electrochemical deposition, although private communications had revealed that there were some attempts. The advantages of an electrochemical approach include: electrodeposition does not require a direct line-of-sight path through the masking material, the nucleation and growth of the deposit can be independently influenced by plating conditions and solution conditions, and electrochemical growth would be occurring in a fluid environment appropriate for a

protein. Some disadvantages involve the larger average grain size of the deposit and the complexity of electrolyte formulations.

What is presented in this work is a new method for nanofabrication via proteins which, given maturation, could lead to integration in solid state devices as a platform for communicating to patterned nanomaterials at densities higher than that which can be achieved by lithography. The goal in this work is to clearly demonstrate that proteins are effective masks, especially in contexts where electrochemical deposition provides unique advantages in terms of bottom-up filling in a fluid environment. Some key challenges that are to be expected will include figuring out which proteins will make good candidates to illustrate the principle as well as survive in the strong ionic solutions characteristic in electrodeposition, achieving the high nucleation densities of material required to fill the protein void spaces, and most importantly obtaining any detailed information about the structure of the deposit at the length scales of proteins in all three dimensions.

CHAPTER 1

Proteins as Pattern Generators for Electrochemical Fabrication

SUMMARY

Bacterial cell-surface layer proteins, or "S-layer" proteins, from three organisms – *Deinococcus radiodurans*, *Sporosarcina ureae*, and *Desulfurococcus mobilis* – were chosen as pattern generating masks for electrochemical fabrication. The proteins have unit cell geometries of 18 nm hexagonal, 12 nm square, and 18 nm square respectively. The S-layer proteins from both *D. radiodurans* and *S. ureae* contain internal structure within the unit cell and therefore permit finer and denser patterns than their lattice constants might otherwise suggest. The proteins chosen ranked in difficulty of use from extremes in simplity to unknown because of a combination of factors related to the growth and harvesting of the host organism, the purification of the protein, and ultimately, the stability of the protein to electrochemical solutions used for deposition.

1.1 From Data in the Literature to Proteins in the Bottle

1.1.1 Introduction

Proteins are a subset of polymers, *i.e.*, a linearly bonded sequence of amino acids with an extra carbon atom in between the amine group and the carboxylic acid group, and this extra carbon atom is where all the functional side groups are attached in a specific order along the chain. Self-assembly is accomplished spontaneously, or by the aid of other proteins whose function is to assist in this endeavour. By contrast, the modern chemical equivalent is that of liquid crystals and block copolymers, where a molecule contains immiscible domains, ensuring phase separation on the length scale of the molecule. This gives rise to a classical set of mesophases which can be classified according to a common series of types depending on the environmental conditions as shown in Figure 1 (taken from a review by P. Ekwall, *et al.* [16]):

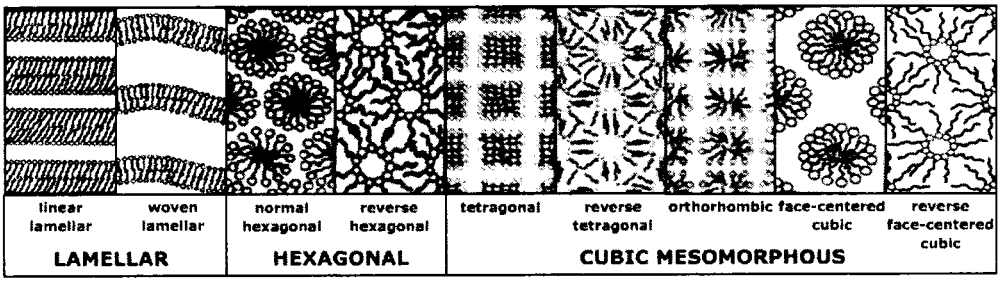

Figure 1: A summary of mesophases available in liquid crystal systems.

Block copolymers are essentially larger versions of liquid crystals, where the length scales can be selected by changing the chain length of the immiscible portions of the molecule. For example, one example system used for fabrication is polystyrene-b-methylmethacrylate, or P(S-b-MMA), where after assembly (often in hexagonal phase and aligned in an external electrical field) the PMMA, being ultraviolet

sensitive, can be removed after exposure to radiation, leaving behind patterned cylindrical holes of a selected size.[17] The essence of obtaining a chosen pattern relies heavily on the choice of chain lengths and, in either liquid crystals or block copolymers, the concentration, nature, and number of solvents involved in preparation, *i.e.*, a phase diagram is needed.

Some polymer chemists, in an effort to break free from the traditional phases, make more complex polymers by adding more blocks to the polymer with different chemistries. Thus, instead of X-b-Y, we get X-b-Y-b-Z and so on and sometimes new forms can be created that do not fall into the classification scheme as shown in Figure 1. If one follows this trend to its ultimate extreme, one might conclude that the greatest level of control over molecular structure is one where every "letter" on the polymer chain is "written" in a well-defined order, *i.e.*, precisely what nature does with proteins using 20 different "letters", or amino acids. Figure 2 is an example of a protein used in this work where its amino acid sequence, obtained by J. Peters, *et al.*, [18] is shown alongside its surface topography, obtained by D. J. Müller, *et al.*[19] This structure is the product of the sequence and does not rely on environmental variables, although aggravating conditions may potentially damage it as will be discussed later in this chapter. Thus, unlike previously mentioned self-assembling systems, the final structure of a protein is *genetically encoded* and *naturally synthesized*; it is therefore fixed, permitting a very useful, highly accurate template, or mould, for fabrication at molecular dimensions.

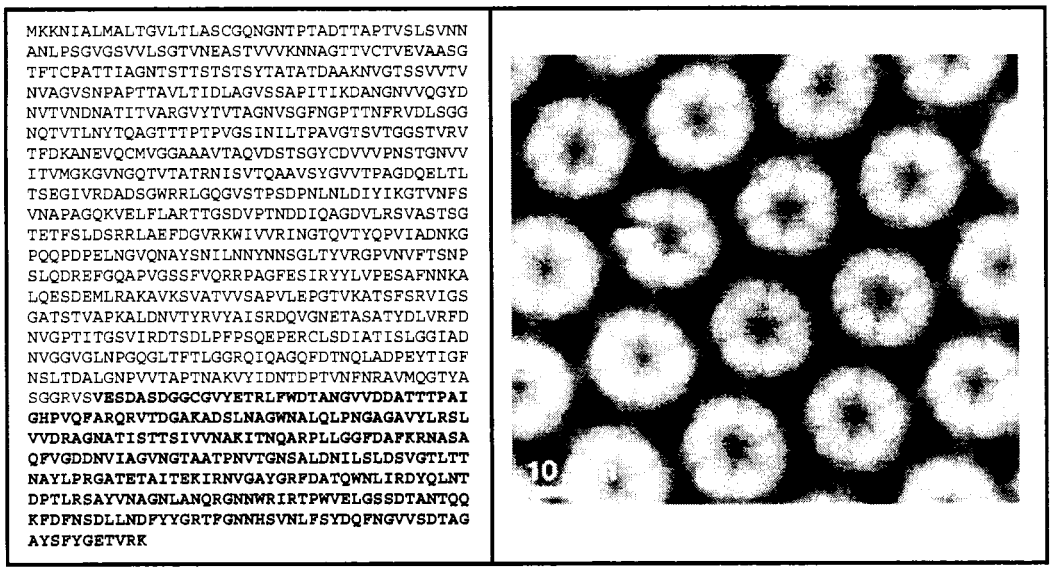

Amino acid sequence of the protein

Atomic force microscopy of the protein crystal.

Figure 2: The cell surface protein of *Deinococcus radiodurans*: Sequence and structure.

Fabrication around the extremely small spaces between and inside protein molecules requires a very high fidelity nucleation and growth strategy. Because this work is focussed on building on surfaces for the purpose of eventually being able to communicate to the structures made, the challenge is multiplied by the vagaries of heterogeneous surface energies which will require a careful selection of the surface and its consideration as part of the fabrication process. The previously mentioned work involving preformed nanoparticles does indeed allow one to construct precise particles, but filling the protein volume and contacting the surface may not always follow. Vapor deposition mechanisms are severely restricted by the protein coverage and the openness of the pore structure. Salt precipitation is an electroless mechanism which will perhaps perform a good job of filling the space, but control over which parts of the protein are nucleated will be governed by the residues responsible for nucleation and reduction of the salt, if needed, will be an additional step. Both vapor deposition and salt precipitation have been useful for visualization since the 1940's and 1950's,[20, 21] but were not used as fabrication tools. An aqueous electrodeposition mechanism, which is the goal of this work, would begin nucleation

on the surface, ensuring electrical contact, but from there, proceed to fill space volumetrically even underneath confined spaces so long as ionically accessible space is available. Electrodeposition offers the combined advantages of a surface-confined nucleation mechanism, a volume-filling growth mechanism, and the convenience of operating in fluid environments under environmental conditions likely to maintain the structural integrity of proteins. Perhaps its greatest drawback is the complexity of electrolyte formulation and the need to consider both electrode surface and electrolyte volume as integral to the fabrication process.

Except for some commodity enzymes and specialty proteins, most proteins cannot be purchased from catalogues. A typical commodity enzyme is egg-white lysozyme, a digestive protein which can be purchase inexpensively as crystals in bottles. Specialty proteins which come in small ampules would include proteins such as bovine serum albumin (BSA) used as a protein mass standard, and a wide variety of restriction enzymes, proteins that "cut" DNA (deoxyribonucleic acid, the genetic chemical that encodes each life form) at specific sequences in a specific manner. However, these are not necessarily the kind of proteins that make great patterns for fabrication such as in Figure 2.

By using proteins that crystallize in only two dimensions, we ignore many possible ways which the protein can organize on a surface and limit it to "up" and "down". Additionally, some proteins remain inside the cell, some are retained in the cell wall, some sit on the cell wall exposed to the environment, and some proteins are just routinely exported into the environment altogether. This presents quite a range of challenges in terms of purifying the proteins, from very simple to potentially difficult. Additionally, some protein crystals will spontaneously crystallize once freed from the cell, some will need to be recrystallized under special conditions, and some are purified as intact crystals. Again, the challenges are variable. Some proteins come from microorganisms that are pathogens to either humans or to animals and may

require special laboratory space to work with, which may or may not be a consideration, and some microorganisms require controlled environments. Alternatively, some of the proteins come from plants and some from animals. All these must be weighed against each other when a choice is being made.

Despite these many variables, there does appear to be a good general platform that can be picked out as more likely to be useful than the rest. Table 1 on the following page contains a summary of proteins that organize into 2D periodic arrays. From the many that exist in the literature, this a short list which only contains those whose structures have been looked at in some detail as noted by the reference. Note the prevalence of proteins referred to as "S-layer proteins". Many microorganisms carry on their outer cell walls a periodic protein coating which is generally called an S-layer protein, though this should not be construed to mean there is a common ancestral form from which they have evolved.[22] The S-layers are exposed to the lipid-like cell wall on one side and the aqueous environment on the other, which generally means there is a "sidedness" which may prove useful when coating surfaces. Many can be isolated as intact crystals, and many display unusually high tolerance to temperature and aggressive chemicals.[23] Because of these many properties, bacterial cell-surface proteins (S-layers) are the epitome of convenience and will be the focus of the work contained herein.

Table 1: A variety of 2D protein crystals, organized by structure, whose structures have been investigated.

symmetry	space group	unit cell (angstroms)	protein	source	reference
oblique	p1	64 x 52,121°	Na,K-ATPase	rabbit kidney	[24]
	p1	120 x 29, 93.7°	cell sheath protein	*Methanospirillum hungatei*	[25]
	p1	103 x 79, 81°	S-layer protein	*Bacillus stearothermophilus* NRS 2004/3a	[26]
	p1	94 x 74, 80°	S-layer protein	*Bacillus coagulans* E38-66	[27]
	p1	200 x 380, 82°	S-layer protein	*Chlamydomonas asymmetrica*	[28]
	p1	280 x 210, 88°	S-layer protein	*Clamydomonas angulosa*	
	p1	250 x160, 71°	S-layer protein	*Chlamydomonas incisa*	
	p1	215 x 70, 80°	S-layer protein	*Chlorogonium elongatum*	[29]
	p2	161 x 241, 84°	photosystem II	barley *Hordeum vulgare viridis zb*[63]	[30]
	p2	101 x 78, 91°	vacuole membrane protein	bean seeds (*Phaseolus vulgaris*)	[31]
	p2	285 x 236, 80°	S-layer protein	*Chlamydomonus reinhardi*	[32]
	p2	118 x 78, 73°	S-layer protein	*Aquaspirillum putridiconchlyum*	[33]
	p2	240 x 160, 109°	S-layer protein	*Lobomonas piriformis*	[25]
	p2	118 x 53,102°	S-layer protein	*Lactobacillus acidophilus* ATCC 4356	[34]
rectangular	$p12_1$	138 x 145	photosystem I	*Synechococcus* sp	[35]
	p2gg	190 x 176	C-reactive protein	rabbit serum	[36]
	$p2_12_1$	73 x 184	catalase	beef liver	[37]
	$p22_12_1$	100 x 79	OxlT	*Oxalobacter formigenes*	[38]
	$p22_12_1$	71 x 81	OmpG	*Escherichia coli*	[39]
	$p22_12_1$	111 x 122	Omp21	*Comamonas acidovorans*	[40]
	$p22_12_1$	182 x 154	BetP	*Corynebacterium glutamicum*	[41]
square	$p12_1$	157	Potassium channel protein	rat brain	[42]
	p2	97	S-layer protein	*Pseudomonas avenae*	[43]
	p4	128	S-layer protein	*Sporosarcina ureae*	[33]
	p4	125	S-layer protein	*Aeromonas salmonicida*	[44]
	p4	184	S-layer protein	*Azotobacter vinelandii*	[45]
	p4	115	S-layer protein	*Clostridia thermosaccharolyticum*	[46]
	p4	131	S-layer protein	*Bacillus sphaericus*[a]	[47]
	p4	120	S-layer protein	*Aeoromonas hydrophila* TF7/U14	[48]
	p4	100	S-layer protein	*Bacillus polymyxa*	[49]
	p4	110	S-layer protein	*Pseudomonas acidovorans*	[50]
	p4	90	S-layer protein	*Bacillus cereus*	[51]
	p4	65	S-layer protein	*Pseudomonas delafieldii*	[52]
	p4	65	S-layer protein	*Pseudomonas facilis*	
	p4	64	lens major intrinsic protein	ovine lens fiber cell	[53]
	p4	104	glycerol uptake facilitator (GlpF)	*Escherichia coli*	[54]
	p4g	99.2	CHIP28	human erythrocyte membranes	[55]
	p422	90	heat shock protein	*Mycobacterium tuberculosis*	[56]
	$p42_12$	165	p10	ϕ29 bacteriophage	[57]
	$p42_12$	96	aquaporin 1	human erythrocyte membranes	[58]
	$p42_12$	95	aquaporin Z	*Escherichia coli*	[59]
hexagonal	p3	62	purple membrane	*Halobacterium halobium*	[60]
	$p32_1$	167	H^+-ATPase	*Neurospora crassa*	[61]
	p321	129.5	light-harvesting complex	plant cells	[62]
	p312	162	chaperonin TF55	*Sulfolobus solfataricus*	[63]
	p31m	72	OmpF	*Escherichia coli*	[64]
	p6	80	outer membrane protein	*Bacteroides bucchae*	[65]
	p6	180	S-layer protein	*Deinococcus radiodurans*[b]	[66]
	p6	235	S-layer protein	*Caulobacter crescentus*	[67]
	p6	153	S-layer protein	*Methanoplanus limicola*	[68]
	p6	175	S-layer protein	*Chlamydia trachomatis*	[69]
	p6	256	S-layer protein	*Lampropedia hyalina*	[70]
	p6	146	S-layer protein	*Clostridia thermohydrosulfuricum*	[46]
	p6	145	S-layer protein	*Aquaspirillum serpens*	[67]
	p6	185	S-layer protein	*Acetogenium kivui*	[71]
	p6	311	S-layer protein	*Thermoproteus tenax*	[72]
	p6	304	S-layer protein	*Thermoproteus neutrophilus*	
	p6mm	160	S-layer protein	*Aquaspirillum serpens* MW5	[33]

[a] previously, *Bacillus brevis*
[b] previously, *Micrococcus radiodurans*

1.1.2 Methods and Materials

Stock cultures of cells

Deinococcus radiodurans SARK (ATCC 35073), *Sporosarcina ureae* (ATCC 13881), and *Desulfurococcus mobilis* (ATCC 35582) were obtained as freeze-dried cultures and transferred to 5 mL of growth media: 0.5% peptone, 0.3% yeast extract, 0.1% glucose (TGY medium), for *D. radiodurans*, 3.0% tryptic soy broth (TSB medium), for *S. ureae,* and a complex basal salts medium based on a *Sulfolobus* medium [73] for *D. mobilis* via crimp vials under a nitrogen atmosphere with resazurin as an oxygen indicator based on the protocol by W. Zillig, *et al.*[74] These were grown overnight in rotary shakers at 30°C, except for *D. mobilis* which was grown for weeks at 88°C, and plated onto media solidified with 1.5% agar. Repeated difficulty emerged with *D. mobilis* and so it was abandoned. Individual colonies were regrown overnight at 30°C in the appropriate growth media. Glycerol was added to 24% vol/vol final concentration and 2 *mL* stocks were stored at -80°C in cryogenic tubes.

Cell culture and optical density measurements

For cultivation, a heated platinum wire loop was used to transfer a small amount of cryogenically frozen cells to 5 *mL* of freshly prepared TGY or TSB media, for *D. radiodurans* and *S. ureae*, respectively, and cells were grown overnight at 30°C in

rotary shakers. The overnight culture was used to inoculate 25 *mL* of media (by 50-fold dilution using sterile techniques) and cells were grown to at least early stationary phase. The resulting culture was used to inoculate 1 *L* of growth medium as above. Growth was monitored by measuring the optical density of the solution at 600 *nm* using a 96-well microplate reader with 200 *μL* of sample, with dilution into fresh media as necessary if the density was too high which may result in detecting stray light. To obtain dry cell mass measurements, a known volume of culture was occasionally removed at logarithmically equal intervals of optical density and precipitated at 10,000 *g* and washed by this process repeatedly in deionized water to remove media components before lyophilization. Lyophilization was performed under vacuum for 4 to 5 hours at -50°C to sublimate the ice resulting in a flaky dry cell mat which was weighed on a balance. For obtaining proteins, cells were harvested after early stationary phase and rinsed by repeatedly centrifuging at 2000 to 3000 *g* for 15 min and resuspending in deionized water 3 times.

Protein purification and concentration measurement

S-layer proteins were purified by differential centrifugation. For *D. radiodurans*, cells were stripped of their S-layers by incubation in 50 *mL* 5 wt% sodium dodecyl sulfate (SDS) for 2 hours at 60°C. For *S. ureae*, cells were lysed by a French press operated at 10000 *psi*. In both cases, the suspensions were centrifuged at low speed (2000 to 3000 *g*) to remove denuded and unbroken cells, and the supernatant was

transferred to fresh centrifuge tubes. S-layer proteins were recovered by centrifugation at 28000 *g* for 50 *min*. For *D. radiodurans*, the proteins were resuspended in 2 *mL* 5% SDS and the purification is complete. For *S. ureae*, protein pellets were resuspended in 30 *mL* 50 mM sodium phosphate pH 7.8, supplemented with 1% Triton X-100 and 1 mM $MgCl_2$ (SPBM buffer), and incubated overnight at room temperature. On the next day, S-layer proteins were pelleted by centrifugation at 28000 *g* for 50 *min*, resuspended in 30 *mL* of SPBM buffer and the process was repeated 3 times. Finally, lysozyme (Sigma) was added to 100 $\mu g\ mL^{-1}$ final concentration and the suspension incubated overnight at 37°C in a rotary shaker. Proteins were pelleted and washed in deiniozed water with 1% Triton X-100 three times as above. S-layer proteins from *D. radiodurans* were stored at room temperature in 5% SDS. S-layer proteins from *S. ureae* were stored at 4°C in 1% Triton X-100 and 1 mM $MgCl_2$. Both protein products were stored as stocks at 1 $mg\ mL^{-1}$ concentration based on the Bradford assay [75] using a portion of the protein resuspended in deionized water as the detergent influences the assay results. Bovine serum albumin (BSA) was used as the protein standard in the assay.

Sodium dodecyl sulfate – polyacrylamide gel electrophoresis (SDS-PAGE)

SDS-PAGE was performed essentially as reviewed by D. Garfin.[76] Gels, 1 mm thick, were generally made of 10% or 12.5% *bis*-acrylamide for the resolving gel, and 4% *bis*-acrylyamide for the stacking gel, and operated potentiostatically at 200 V for about 45 minutes using 15 μL of protein samples, which were previously boiled in the running reagent for 5 minutes prior to loading. Staining of gels was performed typically by Coomasie Blue (Sigma) but for quick results copper staining was more often performed.[77]

1.1.3 Results and Discussion

Using modern search engines, one can merely type "2D Protein Crystals" and obtain a vast account of literature dating back dozens of years on studies of proteins that assemble this way. Table 1 contained a partial list of such proteins gathered from from books and review articles, organized by structure, but includes only those proteins whose structure has been characterized in some way along with references. However, this table contains little information needed to choose a protein intelligently, unless one is lucky enough to have friends in a biological laboratory willing to routinely provide fresh protein stocks at regular intervals. Therefore, a table that contains information about how to grow the organism that synthesizes the protein, where it can be obtained, as well as how the protein is purified, is more useful that a mere listing of lattice constants. Table 2 thus contains this additional information on a reduced subset of Table 1 which only contains S-layer proteins. This final table is essentially a more condensed version that has explored the literature deeper to find out key information about how the organisms grow, how the proteins are purified, and if any information has been found regarding studies of their stability in aggravating conditions.

Table 2: A short summary of S-layer proteins containing relevant information for fabrication, including organism growth methods and protein purification procedures.

TARGET STRUCTURE					HOST ORGANISM DETAILS				PROTEIN DETAILS	
unit cell geometry *l* **nm** (x *nm*, β angle)		size [a] *l* **nm**	density [a] *l* #×10^{12} cm^{-2}		Species and Hazard Class (BSL#)		source[b]	growth[c]	purification[d]	stability[e]
p1	10 x 8, 81°	2.8	2.5	[26]	*Geobacillus stearothermophilus* NRS 2004/3a	1	F. Hollaus, Austria [78]	T^+ O_2^- [79]	X RC [80]	D E [78]
p1	9 x 7, 80°	3.0	4.3	[27]	*Bacillus coagulans E38-66*	1	F. Hollaus, Austria	T^+ [72]	L X RC [61] → [72]	?
p2	24 x 16, 109°	6.5	0.8	[25]	*Lobomonas piniformis*	1	CCAP 45/1	ill [25]	DC [81]	?
p2	29 x 24 x 80°	2.5	0.3	[32]	*Chlamydomonas reinhardi*	1	ATCC 18798	ill [82]	L DC [32]	?
p2	12 x 8, 73°	1.8	3.4	[33]	*Aquaspirillum putndiconchlyum*	1	ATCC 15279	common [83]	DC [83]	pH sol M^+ [83]
p3	21	3.8	0.3	[84]	*Sulfolobus shibatae*	1	DSM 5389	T^+ ac [85]	L D DC [86]	?
p3	19	4.3	1.0	[87]	*Acidianus brierleyi*	1	DSM 1651	T^+ S^0 ac [87]	L D DC [87]	D [88]
p4	11	2.0	0.8	[44]	*Aeromonas salmonicida*	2	C. Michel, France [89]	T^- [44]	L DC [89]	?
p4	18	5.4	0.3	[90]	*Desulfurococcus mobilis*	1	DSM 2161	T^+ O_2^- S^0 [74]	L D DC [90]	?
p4	13	1.7	0 8	[91]	*Sporosarcina ureae*	1	ATCC 13881	common [91]	L DC D E [91]	pH M^+ D E [92]
p6	18	3.4	1.1	[66]	*Deinococcus radiodurans* SARK	1	ATCC 35073	common [93]	D DC [94]	pH M^+ D E [95]
p6	18	3.2	2.6	[69]	*Chlamydia trachomatis* TE55	2	F.-F. T'ang, China [36]	inf H DC [96] → [97]	D DC E [69]	D E [97]
p6	24	3.8	0.4	[67]	*Caulobacter crescentus* 15NY106	1	J. Poindexter, NY [98]	common [67]	DC [67]	pH M^+ [67]

a Minimum feature size and areal density is estimated based on the protein structure reconstructions cited in the reference

b **ATCC:** Amer. Type Cult. Collec., **DSM:** Germ. Collec. of Microorg. & Cell Cult., **CCAP:** Cult. Centre of Algae & Protozoa (UK)

c T^+: High T (> 37°C), T^- : Low T (< 30 °C), O_2^-: limited to no oxygen, **Ill**: light, S^0: elemental sulfur required, **ac**: acidic pH, **inf**: infection of tissue, **H**: homogenization of infectant, **DC**: differential centrifugation, **common**: 30° – 37° C, shake flask

d **L**: lysis, **D**: detergent treatment, **X**: chaotropic disruption, **RC**: recrystallization, **DC**: differential centrifugation, **E**: enzyme treatment

e **pH**: pH **sol**: solvent, M^+: solvated cationic content, **D**: detergent, **E**: enzymes, **?**: no significant study known at present

Growth of bacterial cells is conveniently monitored by light scattering, though this data is rarely shown in the literature because one may make alterations to the growth temperature or to media constituents. In general, the literature will cite the stage of growth at which bacteria are harvested, and it will be up to individuals to determine when that time point is reached. Given a recipe for maximizing cell density in a batch fermentor, key growth stages involve the pre-exponential phase, the mid-exponential phase, the early stationary phase, the stationary phase, and the death phase (which is rarely used as a collection point). These stages reflect variations in cell metabolism and, for some proteins, represent opportunities to collect higher yield or higher purity product. From Figure 3, which was collected for both *Deinococcus radiodurans* and *Sporosarcina ureae* as model organisms to be used in this proof-of-concept, one can clearly see the phases and the transition from the exponential phase (which appears linear on a log-plot) to the stationary phase.

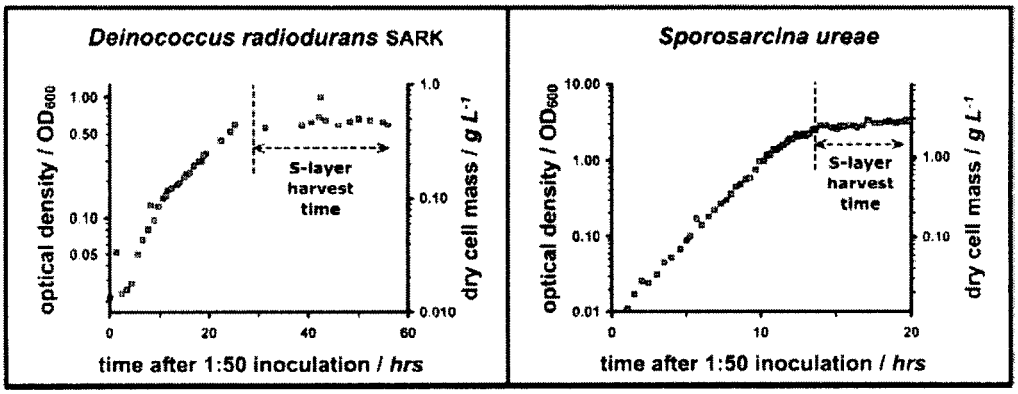

Figure 3: Growth curves (note log scales on the *y*-axes) obtained for *D. radiodurans* and *S. ureae* revealing the time to harvest cells for S-layer protein extraction.

Note the difference in the time taken to get to collection points. The initial point is called the "inoculation", an injection of cells into fresh media from a smaller volume of growth media. The original starting point is a scraping from frozen cell culture in a cryogenic freezer. Also noted is the absence of a growth curve for the organism *D. mobilis*. This archaebacterium (a separate kingdom of life not to be compared equal to eubacteria such as *Escherichia coli* or the others used in this study) is an unusual

archae that grows on elemental sulfur (see Table 2). Although there were numerous studies involved with this organism, [74, 90, 99-104] after contacting the authors it was clear that all cultures were obtained from the original isolator, Prof. Wolfram Zillig, not by following his protocol [74] as often reported. Deeper reading revealed that archae growth on elemental sulfur, due to sulfur's practical insolubility in water, is a poorly understood issue and that these archae might use sulfur in a variety of ways.[31, 105-109] Because of this, it is likely that there is some minor issue with its growth that is not mentioned in the protocol such as a gas needed in the headspace or some other similar thing not thought to be detailed, and so this organism was abandoned. Otherwise, once the growth curve is constructed, harvesting of cells can be performed more casually as most of the time is just waiting (when performed in batch fermentation mode as is done here). Knowing how dry cell mass corresponds to the measured optical density can provide a clue as to how much protein can be extracted if the protein made per biomass of organism is roughly known.[110]

Purification of proteins from harvested cells is often performed precisely as mentioned in the literature, as this procedure often requires a lot of time consuming wet lab work and careful measurements. However, in an article by Baumeister, *et al.*,[110] there was a listing of many variations of the same theme of a purification procedure for the S-layer of *D. radiodurans*. Also, there were subtle differences in other work by P. Lancy, Jr., *et al.*,[95] and B. G. Thompson and R. G. E. Murray,[111] mostly in variations in the centrifugation speeds and whether a true density gradient was used or differential centrifugation was used to separate the cells from their S-layers. In summary, the cells are denser than their S-layer proteins. The S-layer proteins, because they remain crystals, are denser than any soluble proteins. Therefore, purification requires precipitating denuded cells at a low centrifugation speed (the exact speed not being crucial) and removing them. Final purification involves precipitating the S-layers at a very high centrifugation speed (again, the exact speed not being crucial) and removing the solution to resuspend the precipitate

in fresh solution. Figure 4 shows protein gels used to demonstrate product recovery and approximate purity (the contaminant bands are likely cleavage fragments of the original protein, not foreign proteins [112]). So, though normally protein purification is a complex procedure and therefore one often follows the literature religiously, it turned out that, in the case for pre-assembled S-layer proteins, the key issue is to centrifuge the denuded cells at a low enough speed to prevent precipitating S-layers, and to centrifuge the S-layers at a high enough speed to precipitate them all.

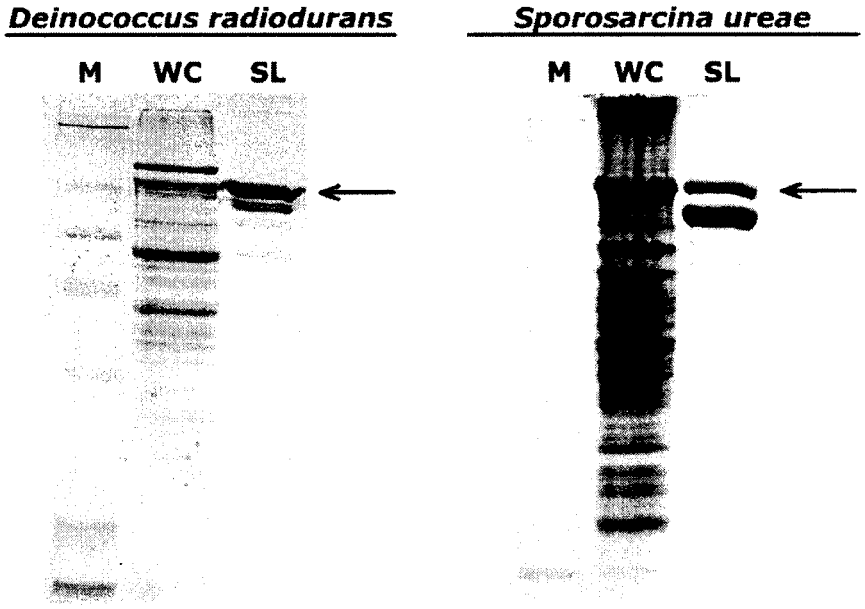

Figure 4: Sodium dodecyl sulfate – polyacrylamide gel electrophesis (SDS-PAGE) patterns of proteins used in this work. Arrow denotes expected position of protein.

M marker proteins
WC whole cell contents
SL S-layers after purification

1.2 Stability of S-Layer Proteins in Electrolytes: The New "Phase Diagram"

1.2.1 Introduction

As seen in Table 2, some S-layer proteins have been subjected to stability studies. The extent of these studies varies, but this data is a good start in finding a good match between a protein and an electrolyte. The types of disrupting agents that are common in these studies are summarized in Table 3 with respective to their relevance in electrochemical fabrication.

Table 3: Summary of common disruption agents used to test proteins in solution and their relevance in electrochemical fabrication

Disruptive Agent	Examples	Electrochemical Application
Alkali Salts	Na^{+}, Mg^{2+}, Ba^{2+}, La^{3+}	Supporting Electrolyte
Metal Chelators	EDTA (ethylenediamminetetraacetic acid)	Stabilizing ligands
Detergents	SDS (sodium dodecyl sulfate), Triton X-100	Wetting Agents
Disulfide Bond Breakers	DTT (dithiothreitol), β-mercaptoethanol	Reducing Agents*
Hydrogen Bond Breakers	urea, guanidine hydrochloride	None known
Enzymes	lysozyme, trypsin, lipase	None known
Temperature	45°C, 60°C, 70°C, 95°C	Common Parameter
pH	2, 4, 7, 10	Common Parameter

* These particular ones are not often used

The work by T. Beveridge [92] looked at the S-layers of *S. ureae* under solution conditions (even most of these here) and characterized their disruption by staining them under a transmission electron microscope. Although this method is good for indicating positive results (*i.e.*, good crystals) it is not clear how they distinguished them from negative results which were not shown directly, nor how one could evaluate "partials". Additionally, there may be variations associated with S-layers adsorbed onto surfaces due to the lower degrees of freedom available. The work on *D. radiodurans* was a bit mixed. In one study [95] stability was based on how much protein was solubilized by exposure to various disruption agents (a subset of those in

Table 3) which would only prove complete destruction of the protein, for which none of the agents were successful. This study would have one believe that the protein might be stable up to a pH of 14 overnight or overnight exposure to EDTA, which is quite remarkable. Another study [110] discusses in more detail about how this S-layer protein may in fact denature but leave its outline intact where pH studies were conducted down to pH 1, but a thorough time investigation was not studied, and characterization was performed using rotary shadowing in a transmission electron microscope, which has a better chance of revealing negative results. In summary, before one can use data on protein stability one must scrutinize the protocol used and determine whether that is relevant to the application intended.

In this work, the intended application for the proteins is for them to maintain their structural detail and long range order once adsorbed onto a surface in a given electrolyte for some period of time. To electrochemically build structures only a few nanometers thick, time scales of minutes are most likely the upper bound necessary. Much of this literature might not capture the needed information, and the mixture of data makes it difficult to standardize the results into a readily interpreted form that can be used to guide choices for an electrolyte, though they did prove helpful in providing a starting point. This is most likely due to the lack of need for data in this form because the concept of S-layer proteins being used in fabrication is only recently being introduced, and this work is the first for an electrodeposition process.

Finding the stability range for a protein of our choice will require experiment because the complexity of proteins does not permit *de novo* prediction, and dynamic simulations of proteins in complex solutions are not readily formulated nor would they be reliable without experimental evidence, even if atomic resolution structure were available for these proteins. Ideally, one should span a range of conditions that should demonstrate a trend to show a behavioral pattern that displays a stability "envelope" which would be comparable to a phase diagram, one which points to

locations in phase space where the protein is or is not an intact periodic template useful for fabrication. Because this a matter of a geometrical structure which may change, and protein structure modulations are on the order of several nanometers, the best tool for characterizing this is one that is most sensitive to surface topography. The atomic force microscope is the most direct way to obtain this information, and although faster and simpler methods were sought after, this method was ultimately chosen to perform this key task.

A new challenge then became apparent, that of compressing about one hundred topographic images into a readily interpretable form that captures the essence of the data without introducing human bias due to subjective expectation and the low data collection efficiency of atomic force microscopy. This requires sampling the surface repeatedly without being able to visualize whether the proteins are intact or not, but still able to find the protein "sheets". Additionally, as the tip shape is convoluted with the image, a region of surface must always be captured in the image as a control to determine whether structural data can be trusted to have attained sufficient resolution to determine whether protein structure is intact or not. Finally, a uniform algorithm must be used which processes the numerical data obtained and tested against controls. Thus, using a "blind" data collection mechanism and a single processing algorithm that operates on all data uniformly to reduce images into a collection of data points, it should be possible to determine a protein stability "envelope" without resorting to showing a montage of images.

1.2.2 Methods and Materials

Surface Preparation

Disks of freshly cleaved mica (5 mm diameter) were coated with 10 nm of platinum in a Gatan ion-beam sputter coater, where growth was monitored using an *in-situ* quartz crystal microbalance monitor. The platinum film had a cobblestone appearance with small grains 2 – 5 nm in size and were very reproducible from preparation to preparation.

Protein adsorption

In general, proteins can be adsorbed at complete coverage or partial coverage. For complete coverage, stocks prepared as in *Methods and Materials* from Section 1.2 were used (*i.e.*, 1 mg mL^{-1} protein concentration) and about 5 – 10 μL were applied by pipette onto the surface. Excess liquid was wicked away and the rest allowed to air dry. The surface was then rinsed in deionized water by repeated immersion and dried under nitrogen or argon. For partial coverage, the concentration was diluted tenfold to 0.1 mg mL^{-1} and 5 – 10 μL were applied onto the surface. The excess was wicked away and after 20 – 40 seconds the surface was rinsed in deionized water several times by repeated immersion and dried under nitrogen or argon.

Protein exposure to disruptive agents

Chemicals were prepared from reagent grade chemicals and the pH was tested using litmus paper. Protein-coated surfaces were then either dipped up-side down on a drop of the solution (for 1 second time intervals) or a drop was placed on the surface (for longer time intervals). After the time interval was up, the liquid was immediately blown dry with a nitrogen or argon gas stream. The surface was then rinsed a few times by repeated immersion in deionized water and dried similarly.

Atomic force microscopy

A Nanoscope III AFM was used for all imaging using DI (Digital Instruments) capture software. AFM was performed in ambient conditions in Tapping Mode® using an open amplitude feedback control loop. Scan rates were nominally set to about 1 – 2 linear $\mu m\ s^{-1}$. Tips were obtained from MI (Molecular Imaging) and had typical resonance frequencies of 350 kHz and tip radii of 10 nm.

1.2.3 Results and Discussion

Atomic force microscopy proved very useful for visualizing the topography of protein crystals which requires no sample preparation effort other than adsorbing them onto a smooth surface, such as freshly cleaved mica. Figure 5 shows examples for the two S-layer proteins used in this work.

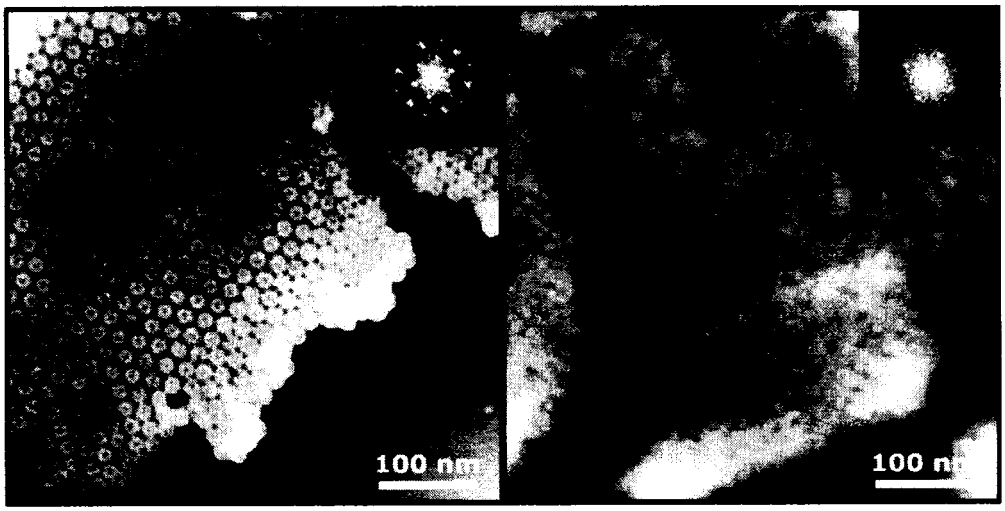

S-layer protein from *D. radiodurans* S-layer protein from *S. ureae*

Figure 5: Atomic force microscopy images of S-layer proteins on mica used in this work

Figure 5 shows these proteins on freshly cleaved mica, excellent smooth surfaces for good detail, but not useful for electrodeposition. The Fast Fourier transform inserts clearly point out the hexagonal and square symmetry involved with *D. radiodurans* and *S. ureae* S-layers, respectively. However, the topography of the *S. ureae* proteins is very difficult to see, and the 3D reconstruction work [91] clearly reveals why this would be so. Thus, work here will be confined to the S-layers of *D. radiodurans*.

A 2D protein crystal can "land" on a surface in only of two ways, "up" or "down". Figure 6 shows AFM images of the S-layer of *D. radiodurans* in both of these configurations.

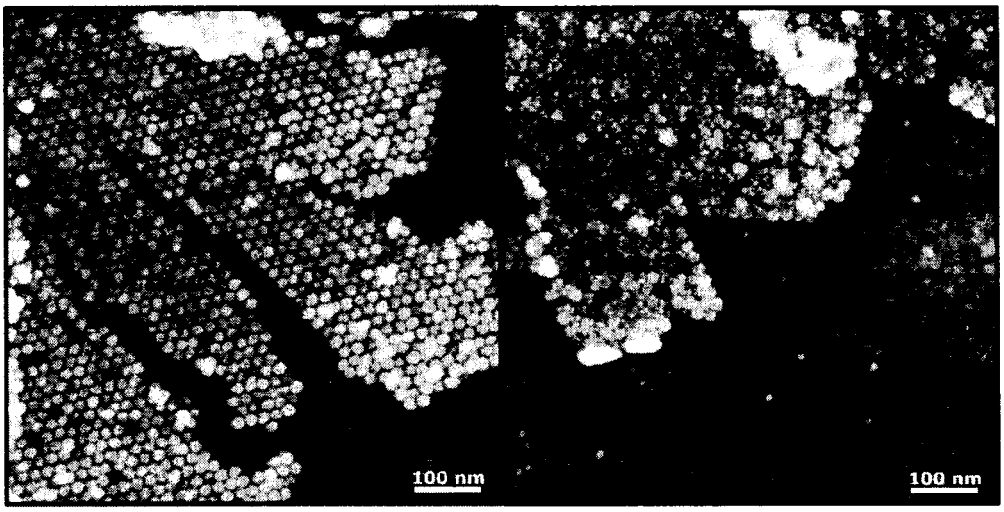

Figure 6: The S-layer of *D. radiodurans* in both "up" (left) and "down" (right) configurations, on platinum-coated mica, noting the difference in topography.

Because of this variation and their potential impact on image analysis, the first step was to quantify how often these proteins expose the "easier to image" side, which we will refer to as the "up" side, over the "more difficult to image" side, which will be referred to as the "down" side. This was performed by repeatedly imaging on the same surface samples of protein crystals. Although we do not show the array of images here, the initial screenings showed that, although perhaps one side may have a preferential adsorption side, the side exposed to the microscope probe is nearly 50-50 "up"-"down" because the protein crystals often fold over, revealing an arbitrary side to the tip which can't penetrate through to the first layer which is the primary template layer for fabrication.

Knowing that, in advance, half of the protein regions are facing in the "down" orientation, the strategy for data capture is to always hunt for folded proteins to guarantee that one always has at least one of the "up" regions in the field of view. This is important because a tip with moderate resolution has shown that a "down" orientation protein can in some cases be misinterpreted as a damaged protein even when no disruption agents were used. Additionally, searching must be performed "blind", that is, without sufficient resolution to see the protein detail but enough to

determine the proteins are there. Figure 7 shows a region captured under "blind" scanning and "capture" scanning.

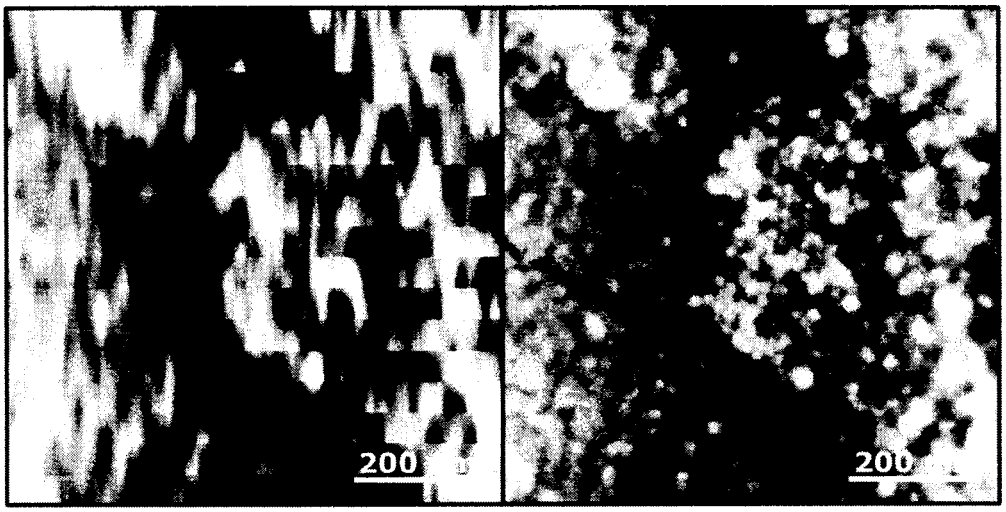

Figure 7: The general strategy for choosing regions for image analysis by AFM to study protein stability in disruption agents. This sample was performed at pH 12 after a 1-s exposure.

Because we wanted to map out a region of conditions that are significant for electrochemical fabrication and see a clear trend that is not sensitive to occassional misinterpretation likely to result from a massive collection of data which is sensitive to these orientation variations, pH was chosen because it is important for both proteins and electrodeposition in aqueous media. As previously noted, the S-layer of *D. radiodurans* was found to be highly insensitive to pH from extremely basic to extremely acidic, but the characterization methods were not uniform nor necessarily applicable to a fabrication technique such as electrodeposition. However, the existence of preliminary work in the literature should allow us to obtain higher quality data to complement these studies and obtain results more useful for fabricators. Figure 8 shows example images used for image analysis under conditions that left proteins intact, partially degraded proteins, and which completely destroyed proteins.

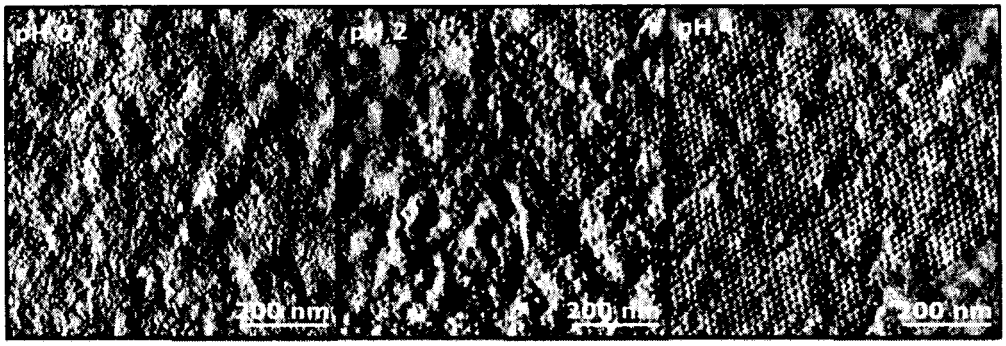

Figure 8: A selected suite of AFM data of proteins adsorbed on platinum-coated silicon taken after the same protein exposure time to different pH conditions. This is a small subset of all data accumulated. The pH conditions are as shown, the time of exposure for all images is 100 seconds. Profilometry across the structures indicate a z height of 5-6 nm, indicating all are monolayers (not shown).

Images were then binned into a "quality" number based on the how much survival there was. For complete destruction a "0" is assigned and for complete survival a "1" is assigned. An automated algorithm became too complex after discovering the issue with folded proteins, so for partials, the data was binned into one-quarter intervals as a discrete quality estimator. The data is plotted versus pH on one x-axis and exposure time on another x-axis, as shown in the accumulated results in Figure 9.

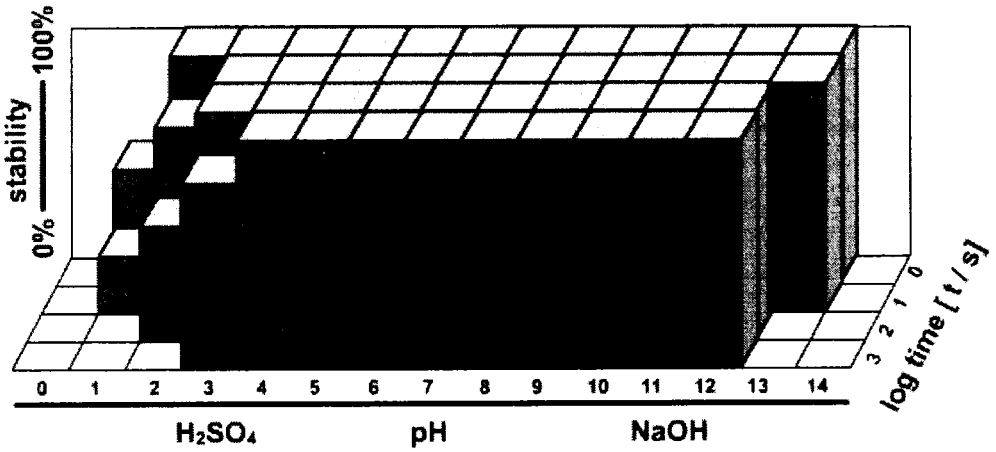

Figure 9: S-layer protein of *D. radiodurans* under different pH conditions for different times. A quality of 1 indicates intact protein crystals, 0 indicates complete disruption.

The combined effect of pH and time is effectively a "charge dose", although we keep them separate in Figure 9 because the physical principle of the disruption may be exceedingly more complex. In principle, a protein has an isoelectric point (pI) about which it will be positively or negatively charged depending on the pH of the solution. Some amino acids such as lysine and arginine will lose positive charge at a characteristic high pH and others such as aspartic acid will gain negative charge. At low pH, the effect will be opposite. Hystidine can exhibit complex charge states which will be dependent on its local environment. Thus, proteins can go through phases where pH has little effect until a critical point is reached, then a massive transformation occurs. Additionally, all proteins are ultimately sensitive to acid hydrolysis, where some peptide bonds are unusually sensitive to low pH due to cleavage of the peptide bond and release of water, but apparently some S-layers have evolved resistance to this. Indeed, many archae thrive in conditions below pH 1, truly a marvel, but protons play a critical metabolic role in some of these organisms' lives, and oxygen is often deadly to them. Their environment-exposed S-layers clearly may have evolved some mechanism of shielding their sensitive peptide bonds from such chemical attack.

CONCLUSIONS

This chapter describes a generic outline for choosing an appropriate protein as an accurate mould, or "mask", for electrochemical fabrication. In summary, books and review articles allow one to find proteins that crystallize in two-dimensions, very useful for fabrication, as well as their lattice parameters. More searching is needed to determine if their three-dimensional structure has been solved to any degree of resolution. Even further searching is required to find data relevant to actually harvesting the organism and purifying the protein for use. Based on this work, it appears that S-layer proteins, on average, are probably the best candidates to work with. This stems from their typically being highly ordered, readily purified, and that some are stable assesmbled in suspension.

Clearly pointed out is that, despite a vast wealth of literature on proteins that organize themselves, there is important information regarding protein stability relevant to fabrication that is not generally available in a readily interpretable form. The work here demonstrates how one can obtain the data oneself experimentally and quantitatively, although this is not likely to be necessary in practice. A more practical approach is to start taking data close to fabrication conditions, and if the proteins do not survive this for the time needed, begin exploring outwards in phase space using less aggressive conditions until the edge of the stability envelope is found. Quantification is not needed if the data is for one's own practical application.

CHAPTER 2

New Tools for Characterizing the Protein-Inorganic Nanocomposite

SUMMARY

In order to use the best tool for characterizing the materials to be fabricated at the length scales necessary, a new platform of self-supported thin metallic substrates were used in conjunction with transmission electron microscopy. These substrates are incredibly thin, *i.e.* 2 – 3 nm, to keep their superimposed detail to a minimum. Because traditional fabrication methods were so tedious but large quantities were needed for experiment, an alternative fabrication strategy is developed to allow a production-scale quantity of these products to be made. Armed with this capability, a vast experimental space can be explored with ease and several applications are shown using the transmission electron microscope and its capability of high resolution imaging, diffraction, and spectroscopy.

2.1 High-Throughput Production of Self-Supporting Thin Metallic Films

2.1.1 Introduction

Electrochemical deposition is essentially a problem of heterogeneous nucleation and growth on surfaces. To fill a nanoscale template well, instantaneous nucleation density must be very high in order to maximize the filling efficiency. Thus, to prove the principle of nanomoulding around proteins, requiring nucleation densities of the order of 10^{12} cm^{-2}, the surfaces will be primarily made of noble metals such as gold, platinum, and palladium, which generally have the highest surface energies for nucleation because their surfaces resist oxide formation.

Perhaps the most challenging aspect of this work is to choose a characterization platform that permits distinguishing the resulting product from other possible nanostructure forming mechanisms. Topography imaging will not say much about the composition of the deposit, and secondary electron imaging in electron microscopes are resolution constrained by the interaction volume of electrons into the bulk of the substrate. The best information can be obtained from an electron microscope and looking at transmitted electrons, but this requires a transmission electron microscope platform, perhaps the most difficult platform as this requires a sample that permits electrons to pass through the sample with minimal scattering. Often, this is achieved by a wide variety of sample preparation techniques, most of which permanently damages the samples and many introduce artifacts,[113] especially when the length scale of interest is a few nanometers arrayed over microns of surface area. Performing this task normally would require sanding the sample from the backside until it is thin enough for grinding, dimpling, and ion milling to transparency. Repeating this on hundreds to thousands of samples is not time efficient.

For others, transmission electron microscopy is relatively simple because the sample is such that it can be captured onto ultrathin films of carbon coated grids which can be purchased commercially. Because of the low surface energy of carbon, it makes a poor substrate for nucleation and growth, and coating an existing carbon-coated grid with a noble metal by vapor deposition requires far too much thickness (nearly five to ten nanometers) before a complete film is formed allowing electrical contact throughout the surface, which has been seen before.[114] The high scattering power of these electron dense noble metals will require an extremely thin film to be made, unfortunately, such products do not exist in the market.

The literature is replete with examples of making metallic thin films.[115-119] Most processes can be generalized as producing a thin coating on a sacrificial support which is then dissolved away after which the film is loaded onto a conventional microscope "grid". This permits one to make several metal-coated grids at a time. Because of the need for repetitive experimentation, alternative strategies were explored, ultimately leading up to a larger-scale preparation method that resulted in a filed patent and allowed the fabrication of over a thousand such products during the course of this study. Sample preparation would thus be eliminated.

2.1.2 Materials and Methods

Sputtering of Materials

A variety of metals were sputter-coated onto sacrificial supports suspended across gold TEM grids (SPI Supplies) such as Sharpie® pen ink, fingernail polish (Revlon®), or a sugar-aerosol solution as described by A. Kuehner.[120] The sugar-aerosol solution is a 2 wt% aqueous solution of sodium dioctyl sulfosuccinate and sucrose added to 40 wt%. Metal was sputter-coated for a film of 2-3 nm thick. Targets used ranged from 60-40 gold-palladium alloy (AuPd), platinum, palladium, gold, silver, nickel, silver, carbon, silica, alumina, copper, and titanium. For AuPd, Pt, Au, Cu, Ti, C, SiO_x, and Al_2O_3, pure targets were used. For Pd, Ag, and Ni, targets were made by electrodeposition of the metal onto a copper target.

Scanning Electron Microscopy (SEM)

Secondary electron imaging was performed on a JEOL 7000 field-emission gun SEM operating around 20 kV at 5 – 7 μA at a working distance of 6 – 10 mm.

Transmission Electron Microscopy (TEM)

TEM was performed typically on a Phillips 420 TEM operating at 120 kV which has an estimated C_s of 1.3 mm. Electron diffraction was calibrated using an aluminum foil standard. Where noted, some work was performed using a JEOL 2010 TEM at 200 kV in the Environmental Molecular Sciences Laboratory at Pacific Northwest National Laboratory (PNNL) with an estimated C_s of 0.5 mm.

Assembly of Nanospheres

Silica or latex beads (Duke Scientic Corporation) were used as obtained and about 1 – 2 μL were applied by pipette onto metal coated grids and allowed to air dry.

Electrodeposition

A traditional three-electrode cell was used in conjunction with a PAR 273 potentiostat/galvanostat in constant potential mode. All potentials are reported to a standard calomel electrode (SCE), *i.e.*, a mercury/mercurous chloride redox system fritted against a saturated potassium chloride solution fritted against the test solution. The working electrode was the metal-coated TEM grid, and the counter electrode was a platinum foil. Copper plating was electrodeposited in an acid sulfate bath, 0.5 M sulfuric acid, 0.5 M copper sulfate,[121] and cuprous oxide was electrodeposited from a Stareck plating bath, 0.4 M copper sulfate, 3.0 M lactic acid, and pH adjusted to 9.0 with sodium hydroxide.[122] Actual plating voltages and times / charges are reported.

2.1.3 Results and Discussion

Using a traditional method, first attempts were made by coating gold-palladium alloy films onto freshly cleaved sodium chloride crystals and then floated off in water for extraction onto microscope grids. A summary of this work is shown in Figure 10.

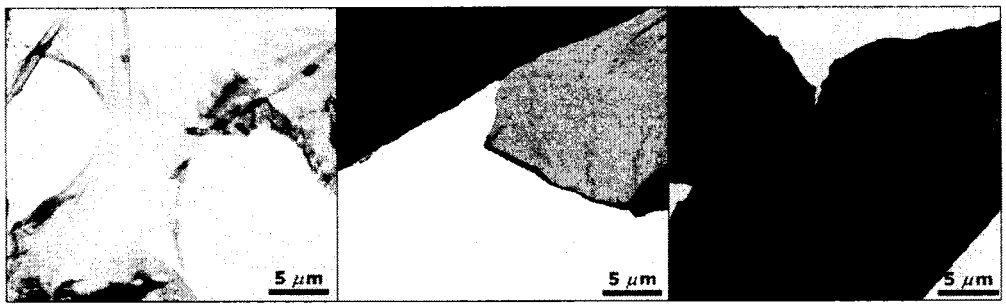

Figure 10: Thin AuPd (60-40) films prepared using the rocksalt technique, various thicknesses. The thickness is not know accurately, so only the relative thickness is shown compared to the thinnest (1x).

Although this did work, it was very difficult to prevent film damage (in Figure 10, damaged films were intentionally chosen for imaging so that empty space could be included in the figure along with the film), and only small regions could be coated. Considering the need for large quantities of such products, the cost needed to be reduced and the quality of product needed to be increased.

Alternative sacrificial materials were then surveyed to find another material that could serve as the base which could act as the receiver of the metal film. Because of the variety of materials tested, such as magic marker ink, fingernail polish, etc., a variety of solvents were exposed to the metal films which later proved to be valuable information. It turns out that water, as an extraction solvent, was resulted in much damage, and that alcoholic media such as methanol and ethanol were superior for maintaining film integrity after extraction. Acetone was reasonable, but the metal films tended to immediately fold upon themselves once freed and when a metal film is folded up it can not be "re-opened". Although it was not clearly understood why at

the time, the ink from a blue Sharpie® pen turned out to be the best alternative; it was cheap, dissolved rapidly and completely in methanol, and the films were rarely damaged after extraction and so were of better quality.

The ink solution worked for some time but this only solved the problem of quality, *i.e.*, it still took significant time to load films floating around in methanol onto grids. A new idea took shape, that if the grid itself could be bathed in the ink in such a way that it could be coated with metal along the ink itself, and the ink could be extracted allowing the metal film to be left on the grid, then a parallel extraction process could be pursued. A platform was needed to allow this and ink was extracted from pens to be applied by pipette onto grids loaded onto a fabricated platform which exposed both sides of the grid to the solvent, allowing the ink to dissolve away from under the grid. Figure 11 shows the platform, where 2/3 of the platter is loaded with grids, and half of the grids have already been "loaded" with ink. The cuts between grid holder spaces allow excess ink to drain away so it does not pile up over individual grids, and the bottom of the platform is cut away to allow drainage of the ink into an alcoholic bath from the bottom side so the metal film stays on the grid. The key to this strategy is that, after the ink dries, there is a solid film left in the grid windows which survives a vacuum and can have metal sputtered onto it. This is Sharpie®'s secret.

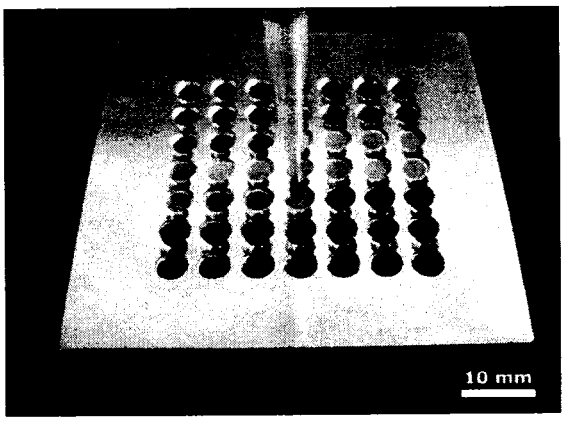

Figure 11: Fabricated grid holder for applying ink into the interstitial spaces inside the TEM grids by a pipette. Note that the next blank grid is just about to have ink applied.

The process yielded an even more exceptional quality of films. The idea of wetting the interstitial spaces between the grid openings was thus born, but the process of doing so still took much time because it still required *handling* individual grids to load the platform and apply the ink. However, once the grids were loaded, every step thereafter was parallel and the time required was independent of the number of grids needing coating. It was also becoming clear that the ink itself had no special properties, that a surfactant that can solidify within the grid windows and survive a vacuum and have metal sputtered onto it will suffice, such as the sugar-aerosol solution introduced by A. Kuehner,[120] but even though it can be dissolved by water, alcoholic solvents were still superior for maintaining film integrity.

The final stage in the evolution of the process required a completely hands-free method for the entire process of obtaining grids onto a loading stage, wetting them with a sacrificial support, coating them with metal, and extraction of the film from the support. Though the fabricated platter was a beautiful piece of machine work, it only serves a few purposes, to allow the sacricial support to make a meniscus between the windows, to expose the grids face up to the coating system, and to provide an underside pathway for the sacrificial material to dissolve away aftwerwards. It was found that the simplest manifestation that could achieve these effects was merely a wire mesh screen that was bent on its edges so that it would be raised above a fluid level. To load grids faster, they could be "sprinkled" from high above a water container where they would float. They could then be manipulated by hand into a small region where the mesh screen could pick up a large batch. The sacrificial support was then loaded onto a dish high up enough that the grids could be contacted to the meniscus from underneath, effectively wetting all of them simultaneously. After a thorough drying of the sacrificial surfactant film, the grids randomly dispersed on the screen was ready. At last, the final process allows the fabrication of an arbitrary number of thin metal film coatings on microscope grids without ever

touching a single one, ready to use in fabrication, where the cost in time and money is very low and nearly independent of how many one makes in a batch. Over a thousand have been made in this work. Figure 12 illustrates this final concept.

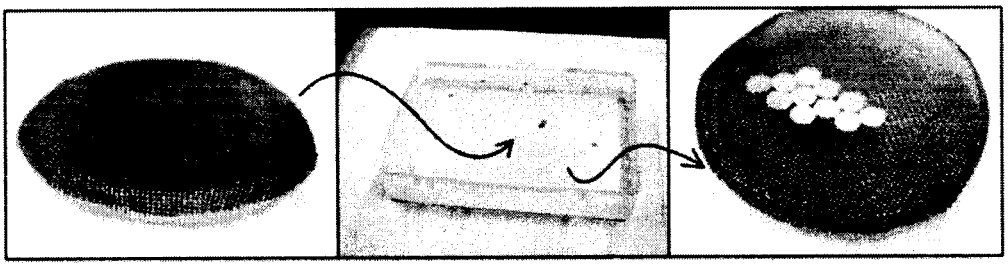

Figure 12: A simple wire mesh screen is enough to load grids and apply a sacrificial support for coating ultrathin metal films in a hands-free manner for high productivity. Here, shown is a copper mesh screen with edges folded over to lift its surface above a fluid level. In the middle image shows some TEM grids (little dots) sprinkled onto a water-filled trough. After moving the grids over to one side by using your hand to confine the grids to a smaller space, they will pack and the lot can be picked up by the holder as shown in the right image. All grids can be coated simultaneously by a sacrificial surfactant film by touching the bottom to a free fluid surface in a dish with a smaller diameter than that of the holder.

The final product is a very thin film containing ultra-fine particles of metal with a "wetting" metal film in between. Figure 13 shows a scanning electron micrograph at low magnification and a transmission electron micrograph at high resolution to show a typical platinum film used for fabrication.

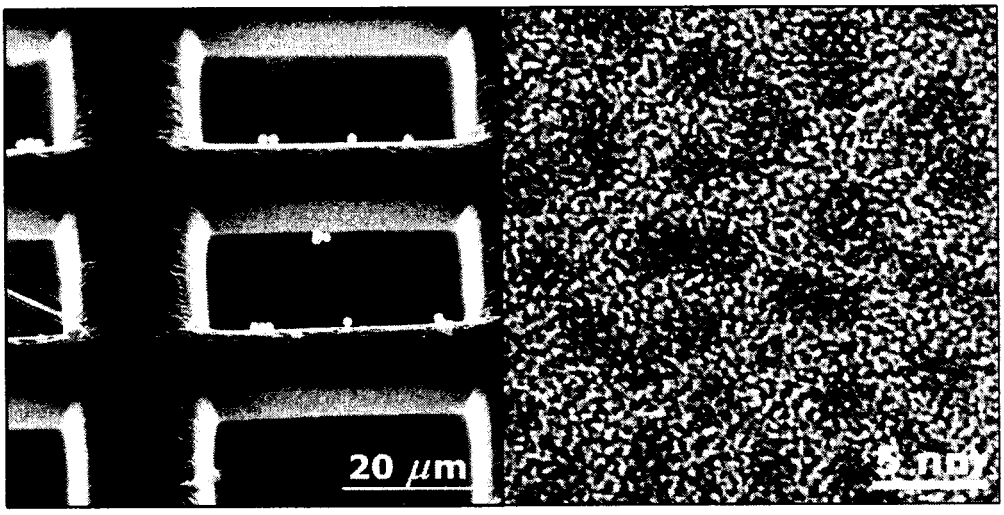

Figure 13: SEM (left) and TEM (right) of a 2 nm self-supported thin platinum film. The TEM was performed at PNNL to obtain the high-resolution structure. The films were loaded with 1.6 μm silica beads to show that there is indeed a surface there.

Demonstrating their value in research, they have been subjected to numerous situations where the surface is a vital component in fabrication, most importantly for electrochemical fabrication. In general, electrodeposition was performed using the method as shown in Figure 14.

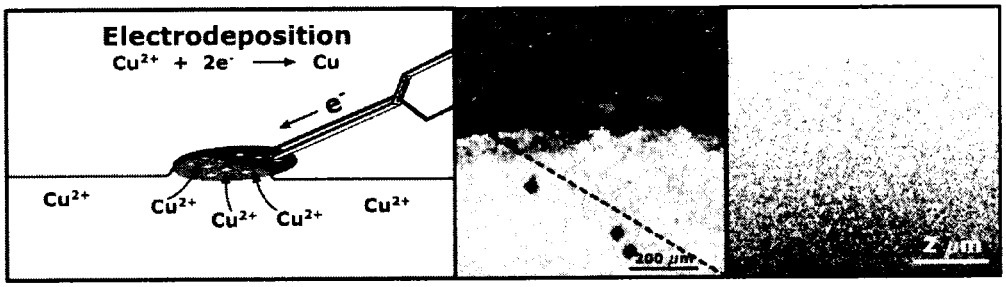

Figure 14: Method for electrodeposition onto the TEM grid working electrode (counter and reference electrodes not shown). The left image is a schematic of the principle. An optical image of the deposit is shown for copper deposition at -300 mV vs. SCE for 3 seconds in the middle, and the far right image is a TEM image of the deposit taken near the interface (dark region is copper, light region is bare platinum).

To illustrate the sample-preparation free nature of this process, a template of polystyrene latex spheres was cast onto an AuPd film, imaged, then electrodepostion of cuprous oxide was performed and the same region was imaged afterwards as shown in Figure 15.

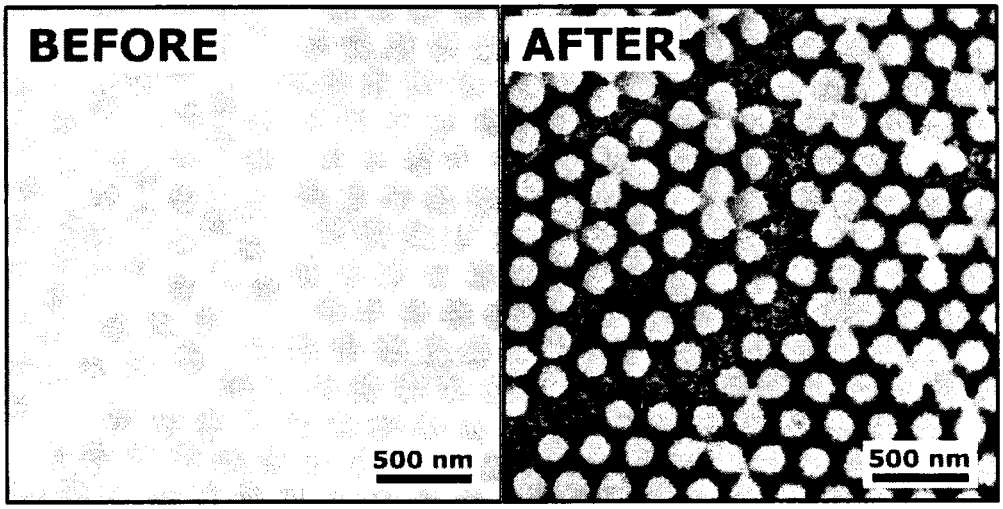

Figure 15: Electrodeposition of cuprous oxide at -450 mV vs. SCE for a total charge to generate about 50 nm of deposit around 240 nm latex spheres, as seen by TEM imaging the same region before and after electrodeposition, on an AuPd surface.

It was concluded that this was an invaluable tool for characterization at the nanoscale templated nanostructures directly on surfaces without the difficulties associated with traditional transmission electron microscopy and associated sample preparation involved with fabricated samples. Clearly, any template could be applied, even proteins, and the many tools that come with transmission electron microscopy, such as diffraction, spectroscopy, and even three-dimensional reconstruction, would become available as will be shown in the following chapter.

CONCLUSIONS

A new platform for plan-view characterization of fabrication processing by transmission electron microscopy is demonstrated which bypasses the need for sample preparation. Although not shown, this platform has also proven useful for self-assembled monolayers, electron-beam lithography, and plasma-enhanced vapor deposition for growing carbon nanofibers. Additionally, the same technique can be used to make many base metal and nonmetal films. A patent entitled "Unsupported, Electron Transparent Metal Films, and Related Methods" was filed with the U.S. Patent Office on Dec. 14, 2005, describes more results with different materials. Some data is also included in the Appendix.

This platform will be crucial to perform the various investigations needed to prove the principle of the electrochemical nanomoulding through proteins concept which will be thoroughly described in the following chapter. This is because of the tremendous variety and high resolution of information attainable in terms of geometry, structure, and composition, available by using transmitted electrons. Very little information was obtained using more conventional nanoscale imaging and characterization techniques, though significant effort was expended.

CHAPTER 3

Proof of Principle: Nucleation and Growth around Protein Void Space

SUMMARY

Using two different S-layer proteins, one from *Deinococcus radiodurans* and the other from *Sporosarcina ureae*, and metal salts of platinum, copper, cobalt, nickel, iron, and palladium, the principle of electrochemical nanomoulding through proteins is proven and generalized. Using the transmission electron microscope in conjunction with electron transparent cathodes, and by keeping the fabrication conditions within the bounds of protein stability, key information about the structure of the deposited material is uncovered allowing for distinguishing the resulting nanostructure from other possible mechanisms such as staining and nanoparticle binding.

3.1 Electrodeposition and Visualization of Nanostructures

3.1.1 Introduction

The peptide bond of proteins is electrically broken by carbons in sp_3 hybrid states, a very poorly conducting bond which should make them insulators compared to the electrode (a noble metal in this study) as well as the depositing material (either a metal or a semiconductor in this study). However, proteins are not merely flat sheets with "holes" drilled into them with a particle beam, but in fact complicated three-dimensional nanoscale architectures which is the reason the term "nanomoulding" is chosen to distingiush these two kinds of mask types. Therefore, it is not possible to employ the "dual Damascene" [123] process used in the microelectronics industry to fill deep trenches with high fidelity, because the internal structure of the protein will be inaccessible to a seed-layer coating. Instead, high instantaneous nucleation density is needed to obtain nuclei at all surface sites exposed at the protein-surface interface and preferably progessive nucleation to fill the volume laterally as rapidly as possible to reach into all the nonconducting crevices before vertical growth overfills the template beyond the desired height.

At electrochemical equilibrium (open circuit), the net current is zero across the electrode interface, though this does not necessarily mean nothing is happening. In principle, there are possibly numerous electrochemical reactions, and the sum of oxidation reactions and reduction reactions simply add to zero. The magnitude of these reactions is called the exchange current density, and is a signature of intrinsic dynamics at equilibrium. To electrodeposit material, the electrode must be biased and the circuit closed at some deviation away from equilibrium, thus electro-deposition is governed by kinetics, where concepts such as mass transfer and reaction rates come into play. When growing such a thin film, the nature of the substrate will also govern the type of deposit formed, and steady-state conditions will not likely ever be achieved. This work will thus always be "in the transient".

Because electrolytes can be tailored so much, there is a potentially vast experimental space to explore. In this work, we focus attention on varying the materials instead of choosing one and tailoring it to perfection. This way, it is hoped that some quality of thin film growth (where thin in this case is on the order of a few nanometers, not microns) and penetration into the cavities of the proteins will be attained, perhaps similar in some ways to the filling of tortuous void space of lead-acid batteries but at a much different length scale. To avoid an explosion of exploration with electrolytes, in this study electrolytes and plating conditions will be chosen because they were either common, studied well in the literature, or provided by commercial vendors.

3.1.2 Materials and Methods

Electrodeposition

Electrodeposition was carried out as in Materials and Methods in Chapter 2.1.2, except for SEM characterization, the working electrode was circular platinum disk of 1 cm diameter, polished down to 0.25 μm with diamond paste. More materials were used, and so all are reported here:

Copper: Strong acid sulfate baths were 0.5 M copper sulfate and 0.5 M sulfuric acid. Mild acid sulfate baths were 0.6 M copper sulfate, 0.5 M magnesium sulfate, pH adjusted to 3 with sulfuric acid. Low concentration copper baths were made with 50 mM sodium acetate/acetic acid buffer to pH 4, 1 mM magnesium sulfate, and 10 mM copper sulfate.

Cuprous oxide: Cuprous oxide baths were made as before, 0.4 M copper sulfate, 3 M lactic acid, pH adjusted to 9 with sodium hydroxide.

Nickel: Nickel baths were based on the Watts type bath, [124] *i.e.*, 1.0 M nickel sulfate, 0.2 M nickel chloride, 0.5 M boric acid.

Cobalt: An ethanolic cobalt bath was selected from the literature based on the work by A. Suzaki and T. Watanabe, [125], 100 mM cobalt chloride in ethanol, and in this case a platinum wire reference electrode was used.

Iron: Iron baths were made with 10 wt% ferrous ammonium sulfate and 10 wt% magnesium sulfate, prepared under argon using

deoxygenated water and electroplated under an argon gas stream with an SCE reference electrode filled with deoxygenated saturated potassium chloride.

Noble Metals: Electrolytes were purchased from Technic, Inc. Platinum baths were formulated from dinitrosulfatoplatinous acid (Platinum AP), silver baths were silver (I) cyanide (Bright Silver), palladium baths were palladium (II) chloride (Pallaspeed), and gold baths were potassium gold (I) cyanide (Neutral Soft Gold).

Preparation of protein templates

Cells were grown and harvested, and proteins purified as in Materials and Methods of Chapter 1, section 1.1.2. Proteins were adsorbed onto metal-coated grids under either partial or complete coverage conditions as described in Chapter 1, section 1.2.2. Metal coated grids were prepared as described in Chapter 2.

Scanning Electron Microscopy (SEM)

SEM was performed as described in Chapter 2, section 2.1.2.

Transmission Electron Microscopy (TEM)

TEM was performed as described in Chapter 2, section 2.1.2.

3.1.3 Results and Discussion

Before a given material is attempted with respect to deposition through protein, its nucleation and growth as a plain film is studied first using conventional electrochemical studies such as voltammetry and electron microscopy. In the absence of literature data, a simple and efficient study involves sweeping the potential from equilibrium towards more reducing until a plateau or a spike is reached. The plateau is indicative of some kind of rate-limitation such as depletion of the ions at the interface (mass transfer effects), limited anode oxidation capacity (often designed to not be a problem), or in the case of p-type semiconductors such as cuprous oxide, the mobility of electrons through the deposit. A spike is indicative of the hydrogen evolution potential, or another secondary chemistry of unintended consequences. A follow-up study will then involve a constant potential deposition at various points along the sweep for the same total charge (over the same area of surface) and imaging in the SEM or TEM to qualitatively look at the nucleation density. The product with the finest grain wins.

Figure 16 illustrates this process using a low concentration copper plating bath which was altered from standard recipes. The voltammetry is only a fast overview since the process is occuring while deposition is happening; we are seeing the effect of nucleation and growth on what was initially a platinum surface then a mixed copper / platinum surface depending on the rate at which the voltammetry is scanned. The rate of the scan will also influence the rate of the depletion of the ions at the surface so the mass transfer limiting current (if the plateau is indicative of this effect and not of something else) appears to be different than it would be if a pulse were applied. Thus, different curves are taken on fresh electrodes, as shown, to look at nucleation behavior under constant potential deposition, where a step potential is applied and held for a given duration. The intial sharp rise is due to electrode charging needed to "build" the electrode double layer, effectively a capacitor that is solid on one side and

an ionic liquid on the other. The small hump, as shown by both arrows in Figure 16, at the smaller overpotential is indicative of an instantaneous nucleation event which is then overtaken by growth on existing nuclei. At greater overpotentials, nucleation can dominate progressively, so the hump is not seen, instead, nucleation occurs rapidly everywhere, and the current transient decays as the double layer is depleted of reacting ions and a concentration gradient expands outward into the bulk solution. If the solution is not mixed well, this is a likely candidate for fractal-like dendritic "arborescent" growth over time.

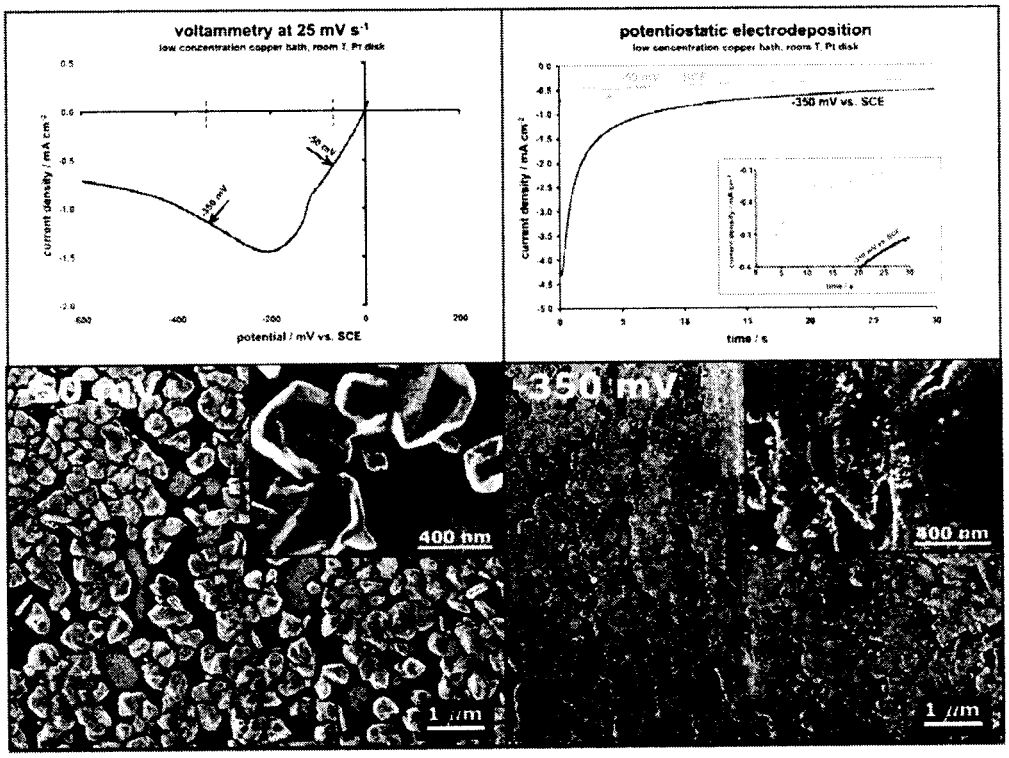

Figure 16: A basic approach for finding conditions for an unknown system. First (upper left) voltammetry is performed to find reaction limiting conditions (such as at -50 mV here for a low concentration copper bath) and what appears to be mass transfer limiting conditions (such as at -350 mV). Next, after repolishing the surface, electrodeposition at constant potential is performed at chosen conditions (upper right figure, insert shows different current range). SEM is then performed on the deposits (lower two figures, labelled depending on conditions, performed for the same total charge, *i.e.*, total mass deposited) to look at nucleation and growth.

In summary, voltammetry provides an *in-situ* overview of nucleation and growth integrated over the entire surface, and electron microscopy provides *ex-situ* the fine detail needed to determine which conditions are likely to generate the density needed to fill protein void space. Another *ex-situ* technique that is useful but not used here would be x-ray diffraction, where the figure of merit to look for is the smallest grain size attainable.

Some of the best quality films were produced using cuprous oxide electrolytes. These were tested extensively on both proteins in this study under both partial coverage conditions (more useful for analytical purposes) and complete coverage conditions (which illustrates the electrochemical principle of bottom-up filling). Figure 17 shows an example of a partially coated AuPd film with cuprous oxide electrodeposited through a protein mask derived from the S-layer of *Deinococcus radiodurans*. The image pair shows both a surface merely coated with protein, and the resulting TEM image of the deposited material on a protein-coated metal film. The high magnification inset in the TEM image is an FFT-filtered image using the most visible spots in the power spectrum as well as the center spot to form the mask for the inverse FFT, showing that on average the pattern of the protein structure is well-preserved in the deposit. Some artifacts appear as a result of the crystals not being in perfect hexagonal lattices. Notice that a plain speckled film of random crystallites forms in regions where patterns aren't evident, indicating that electrodeposition proceeds in all areas regardless of whether a mask is applied. This is useful for analysis as these structures will later be probed and the unpatterned areas are like built-in control samples. The same type of results are shown in Figure 18 for the S-layers of *Sporosarcina ureae*.

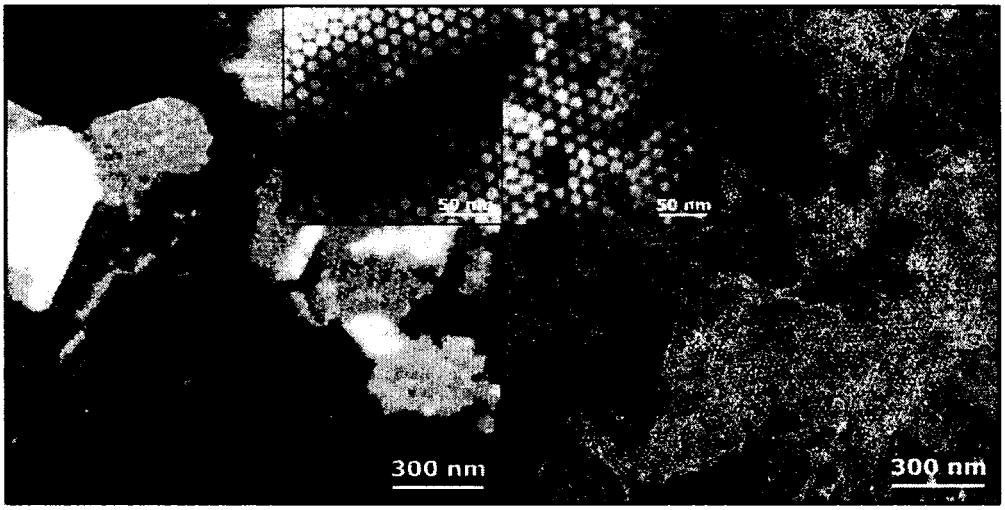

Figure 17: Electrodeposition of cuprous oxide at -450 mV vs. SCE for 10 minutes on AuPd using the S-layers of *D. radiodurans* as the mask. Left image is a topographic image of partial coverage, and the right image is the resulting TEM image of the deposit. In TEM, the protein is essentially transparent (brighter) than the deposit (darker). Also, diffraction produces extra contrast where deposit crystals are oriented with strong diffraction zones normal to the beam, seen as a random assortment of dark speckles in the image.

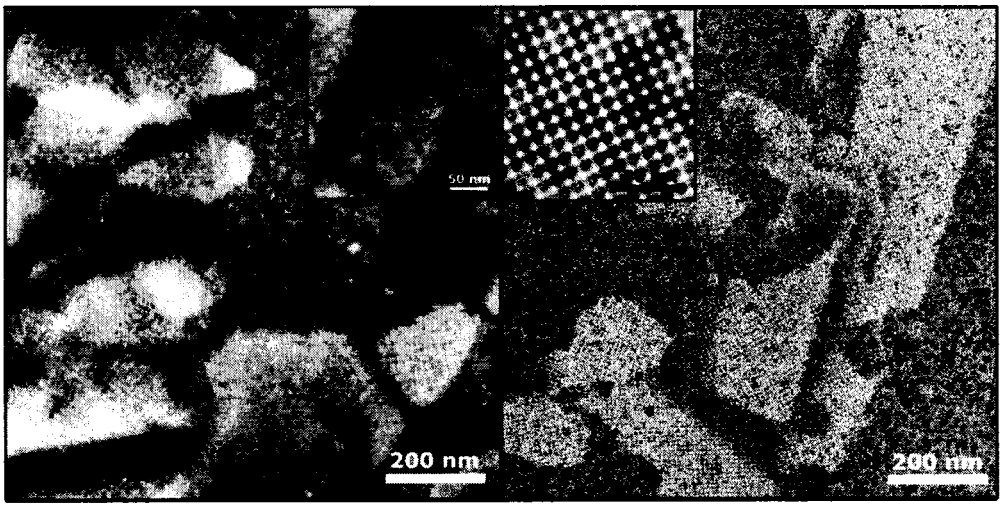

Figure 18: Similar to Figure 17, except electrodeposition of cuprous oxide was performed through S-layers of *S. ureae* on Pt. Otherwise, all conditions were the same.

Figures 17 and 18 show the resulting patterned deposits using proteins studied under partial coverage coverage conditions. With S-layers of *D. radiodurans* the resulting deposit has a pattern geometry of a hexagonal lattice with a periodicity of 18 nm just

like the protein mask, and with S-layers of *S. ureae* the resulting geometry is a square lattice with a periodicty of about 13 nm just like its protein mask. To follow up this study, complete coverage conditions are also tested to demonstrate the capabilities of electrodeposition to reach the electrode through protein multilayers, though these conditions are not further used for analytical work. These are shown in Figure 19.

In each image pair are shown topographs of a fully coated surface and electron micrographs of electrodeposited cuprous oxide performed as before on platinum thin films fully coated, using both proteins studied in this work. Because of the vast height variations in the topographs, they are shown in amplitude mode, *i.e.*, the oscillation response of the tip to the changing topography which generally goes higher (displayed brighter) when going up topography and goes down (displayed darker) when going down in topography (as it scans left to right), which can be be crudely thought of as a surface which is "illuminated" by a light source from the left of the image. In the electron micrographs, the image is a mosaic of the many protein crystals in contact with the surface, and any overgrowth is forced through multilayers. Thus, no filtered image is shown, instead the fast Fourier transform is shown, revealing the many rotated crystals which can join to form rings at the characteristic primary periodicity of the protein crystal selected.

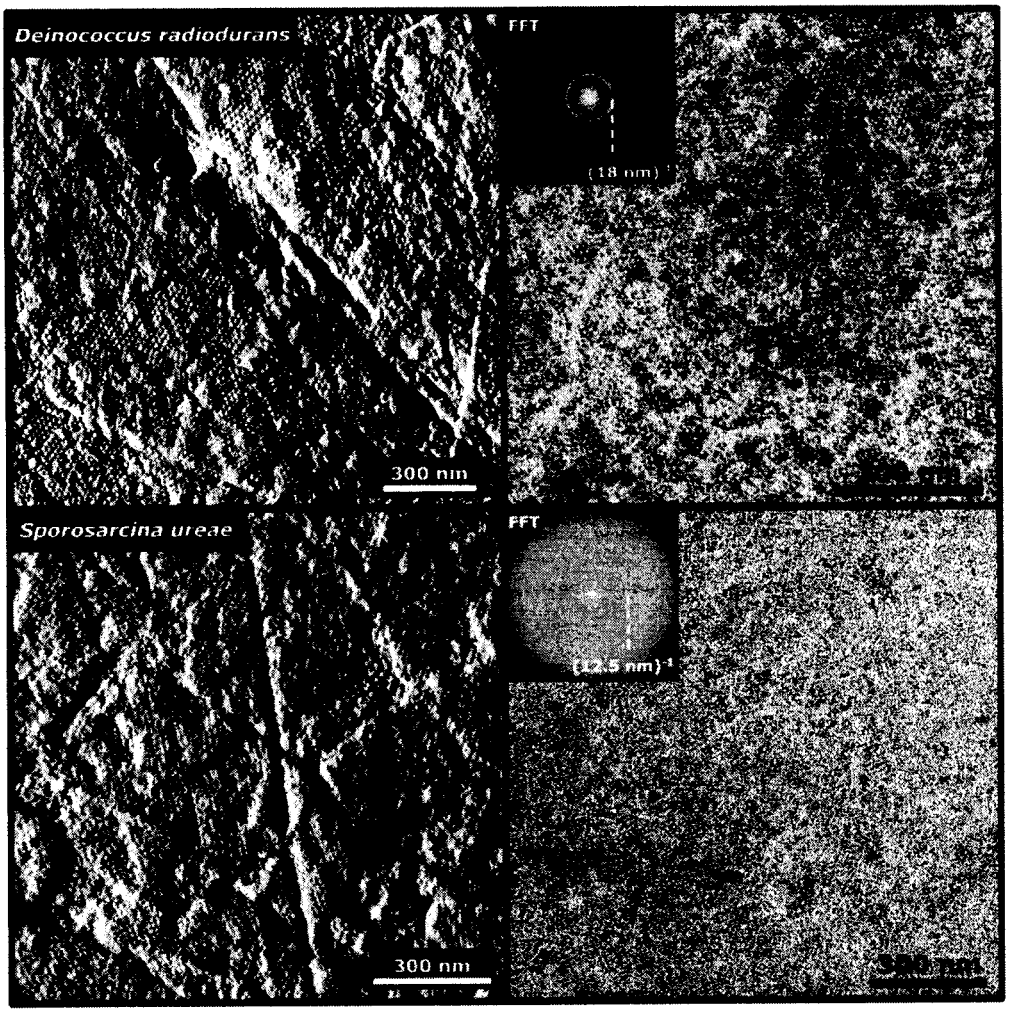

Figure 19: Electrodeposition of cuprous oxide under the same conditions as in Figures 17 and 18 on Pt films under complete protein coverage conditions. Because the surface is completely covered, the topographs (left) are a complex stack of overlapping protein crystals and the image is shown in amplitude mode. The TEM images (right) show a mosaic pattern of many rotated crystals, which shows up in Fourier transforms as rings with a characteristic primary displacement to that of the protein used (labelled on the top left corner of each image pair by its host organism).

To generalize the process to other materials, electrolyte systems for metals were chosen. Figure 20 demonstrates the metals which were successfully patterned through the S-layers of *D. radiodurans*. No success has been achieved thus far with the S-layers of *S. ureae*, and a more thorough understanding of its stability in electrolytes is thus in order. Topographs are not recorded here, as they are all the same as in the sub-monolayer case as in Figure 17, but each electron micrograph is shown alongside its FFT insert in the upper left (with the metal labelled) and a filtered image insert in the upper right.

Each material system has its own characteristics, although to look for trends across materials is a difficult thing to do as the surface, the electrolyte, and the material being deposited all contribute to its structure. One obvious feature are variations in nucleation density, and the variations in deposit morphology. For example, platinum forms very large nodular deposits (in TEM, it seems everything is very large, even though the deposition conditions were carefully selected by voltammetry and SEM for very fine grains as previously mentioned). A possible explanation is the need for high overpotentials to prevent preferential nucleation on freshly deposited material, however, in the case of platinum, its surface energy is such that its nuclei may have surface energies that exceed that of the electrode surface so that once nuclei form, they become preferential nucleation points for growth, making film-like growth very difficult. Applying greater overpotentials to overcome this might be obvious, but the commercial baths appear to be well formulated for robustness against potential variations, so there was little gain in doing so, things only got worse. The best case outside cuprous oxide was for cobalt in an ethanolic bath. Ethanol was used because in aqueous media, highly textured crystals were formed, with large grains (not shown). This makes growth highly anisotropic, not ideal for lateral growth to fill in tortous non-conducting void space. In the literature this ethanolic system [125] was was claimed to produce "amorphous" cobalt, though clearly this means too fine-grained to contribute significantly in x-ray diffraction.

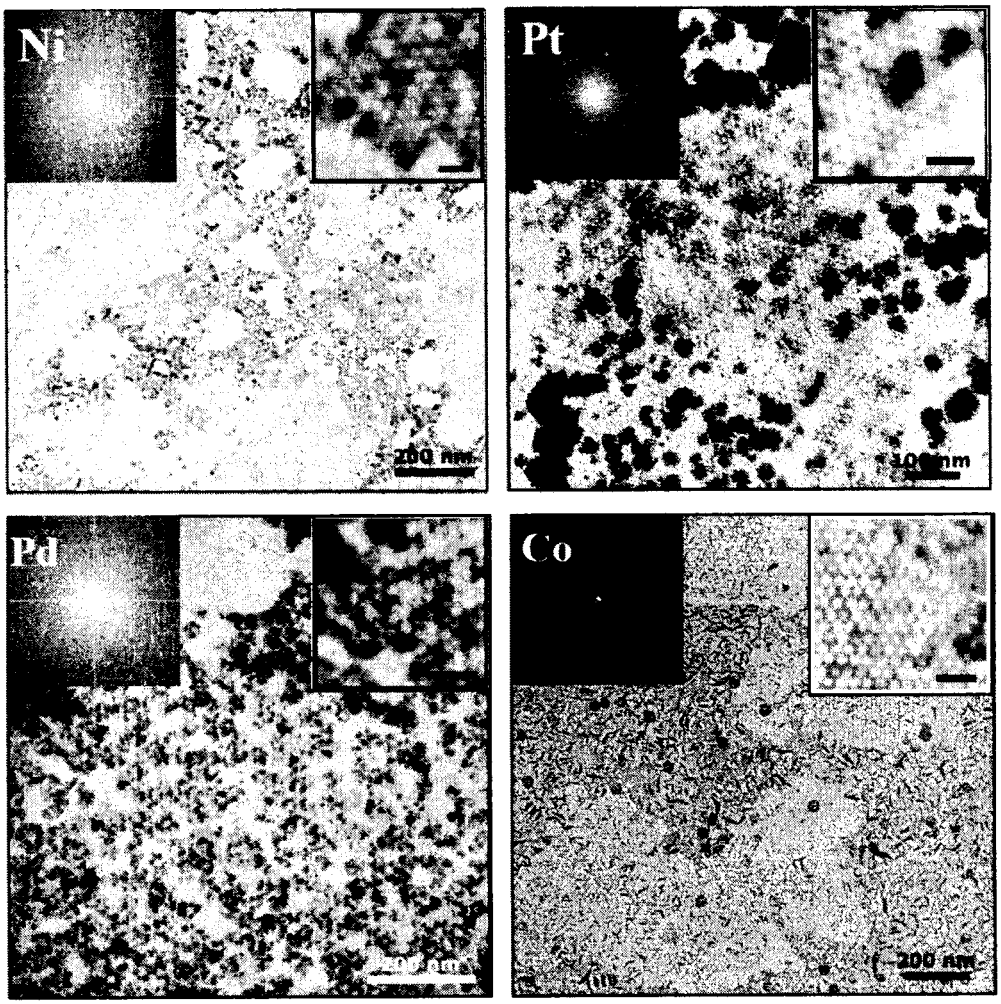

Figure 20: Electrodeposition of various metals through S-layers of *Deinococcus radiodurans* under partial coverage conditions on AuPd films. Ni was plated from a Watts-type bath at -850 mV vs. SCE for 15 s. Pt was plated from a commercial bath at -175 mV vs. SCE for 2 s. Pd was plated from a commercial bath at -900 mV vs. SCE for 5 s. Co was plated from an ethanolic bath at -1750 mV vs. Pt for 30 s. FFT inserts (upper left) are included, with the metal labelled along with filtered images (upper right). All scale bars in filtered images correspond to 50 nm.

For *Sporosarcina ureae*, no base metal system worked for which it is believed to be due to protein instability in acidic electrolyes as described in Chapter 1; however, for *Deinococcus radiodurans*, a very wide range of materials could be nanostructured with the noted exception of copper. Under a failure, what is seen are empty regions of geometric patches surrounded by deposited material, and close examination reveals no material within the electron transparent space, except perhaps a few scattered nucleated deposits. Based on knowledge obtained in Chapter 1, section 1.2, it became obvious that a strong acid sulfate bath was the source of this failure. Essentially, at a pH of 0, the protein pattern is immediately lost in less than a second, although the protein sheet is still physically on the surface. Thus, the first, and only apparent needed adjustment was to move the pH towards a more compatible region for the needed time. For copper plating, barely a few seconds of time is needed for exposure to electrolyte and plating, so a mild acid sulfate bath at pH 3 was made, and to maintain ionic strength magnesium ions (of sulfate) were substituted for the loss in protons. The results are shown in Figure 21.

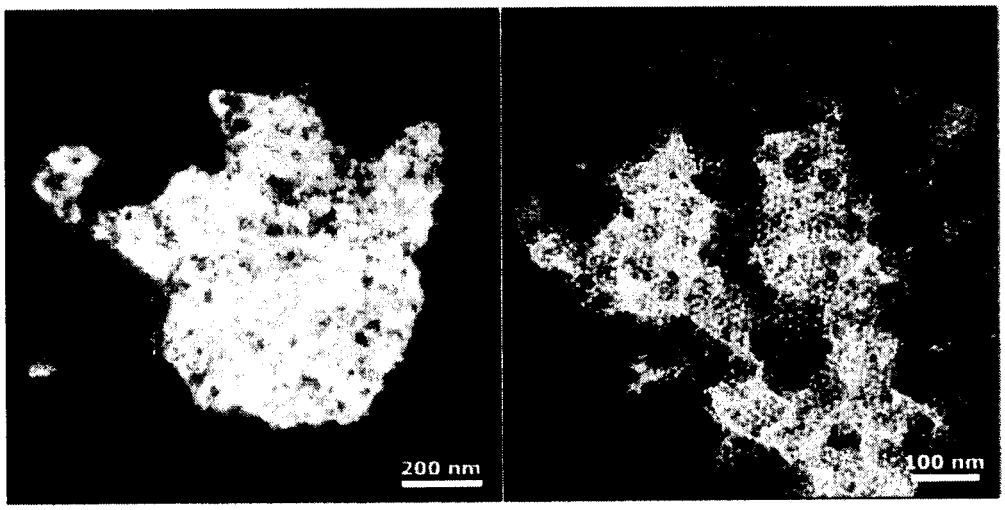

Figure 21: TEM images of copper electrodeposition on Pt at -300 mV vs. SCE for 3 s through S-layers of *D. radiodurans* under partial coverage conditions. The left image was done using a strong (pH 0) acid sulfate bath, the right image was done using a milder (pH 3) acid sulfate bath supplemented with Mg^{2+} to maintain ionic strength.

3.2 Electron diffraction studies

3.2.1 Introduction

Although Chapter 1 discusses the stability issue of proteins with respect to pH, it does not address the complexity of electrolytes which will also contain background electrolytes, high concentrations of metal salts, and potentially additives such as wetting agents and metal chelators. Thus, pattern formation in the TEM can accompany the mere exposure of an electrolyte to proteins, or follow an electroless reduction pathway as a result of the presence of oxygen, or a change in pH near the cathode. Although the TEM image itself contains diffraction phenomena such as diffraction contrast, electron diffraction is the most direct way to confirm the presence of crystalline material which is the product of an electrodeposition process, and readily distinguishes between salts, oxides, and pure metals. Unlike x-ray diffraction, electron diffraction can easily sample regions from nanometers to many microns in size which can be directly connected to its electron image.

One disadvantage of diffraction analysis is that, while a crystal structure has only one true electron diffraction pattern, an electron diffraction pattern does not identify a unique crystal structure. An energy-dispersive spectroscopy detector (EDS) or electron-energy loss spectroscopy detector (EELS) can provide the elemental analysis if desired to narrow down the list of possible structures, but in most cases the critical piece of data is the electron diffraction pattern. This will be the case here because electrodeposition generally provides such pure phases that unless the structure matches that expected, one can consider the process to have failed. If failure occurs repeatedly, then the elemental analysis may prove more valuable to identify the failure mode, or where the structure of interest is not an inorganic crystal such as the protein itself (electron crystallography of protein crystals is an endeavor unto itself).

3.2.2 Materials and Methods

Preparation of Samples

Samples were electrodeposited through S-layer proteins prepared as detailed in Chapter 1 in section 1.1.2 under partial coverage conditions as described in Chapter 1 in section 1.2.2 on self-supported metal films made as described in Chapter 2 using the methods as described in this chapter in section 3.1.2.

Transmission Electron Microscopy

Transmission electron microscopy was performed on a Phillips 420 TEM at 120 keV as described previously in Chapter 2 in section 2.1.2.

Electron Diffraction

Electron diffraction was performed using a nominal camera length of 950 mm, with an effective camera length adjusted by calibration with an aluminum foil standard. Parallel beam diffraction patterns were used in conjuction with a selected area aperture to define a circular region of interest, with a minimum selectable diameter of 1 μm. Converging beam diffraction was used to examine crystallinity of individual particles, with the smallest useful probe size of 3 – 5 nm, depending on the material.

3.2.3 Results and Discussion

In all experiments, sub-monolayer coverage conditions were chosen to ensure that on the same sample, regions of plain film could be compared side-by-side with regions containing patterns as a built-in negative control. In some cases, bare areas could be found nearby, due either to surface contamination by adventitious carbon or sometimes to the excessive resistivity of the film due to its being extremely thin. These regions are very useful as a third control, *i.e.*, regions that contain a three-phase interface, where there is no film, plain film, and patterned film all in one field of view. This allows electron diffraction due to the substrate to be sampled independent of the material deposited, despite its weak signal. Figure 22 shows an example of one such interface for cuprous oxide electrodeposited through the S-layers of *D. radiodurans*.

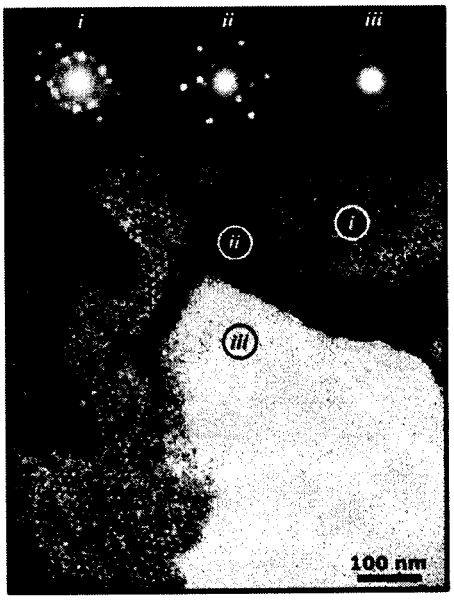

Figure 22: Converging beam electron diffraction of cuprous oxide electrodeposited at -450 mV vs. SCE for 10 minutes on AuPd through S-layers of *D. radiodurans*. Above the image are the diffraction patterns of the regions shown in circles: (*i*) patterned film, (*ii*) plain film, and (*iii*) bare surface.

Interpreting the converging beam diffraction patterns shown in Figure 22 takes a bit of time. Essentially, one assumes a crystal structure (such as cuprite, the crystal structure for cuprous oxide and one other material, silver oxide), and finds a pattern of spots that appears grouped together (such as the hexagonal series in the plain film region). The spots are then indexed using a software package which checks your measured displacements and angles (taking into account the accelerating voltage and the calibrated camera length) and provides a list of possible crystal orientations. If one appears suitable because the intensities of the spots match well, then the match is likely. One must also check other possibilities, such as cupric oxide (CuO, vs Cu_2O), and copper (Cu), etc. However, both patterns index to Cu_2O and the bare surface clearly indicates a significant loss of crystallinity relative to the film regions.

A contrasting example is that of gold deposition from a commercial gold cyanide bath. The result is shown in Figure 23. The figure shows an attempt to electrodeposit gold through the *D. radiodurans* S-layers on AuPd. At first the presence of a pattern was heralded as a success, however, after attempting electron diffraction, where local analysis was needed because the structure of pure gold differs from the substrate (a gold-palladium alloy) by only a trivial amount, it could not be determined to be gold. Although some spots happened to be at the right position, the pattern does not index to any orientation of a gold lattice. Another indication that this is not an electrodeposition product is the lack of crystallites surrounding the patterned region. Thus, electron diffraction proved invaluable in scrutinizing the results because one can ask what the compound is. Because of the electron density, there is almost certainly gold there, but it probably is a precipitate of some kind. Later, it was discovered that the detergent used to store the proteins is incompatible with cyanides, resulting in a white precipitate, regardlesss of the direction of dilution (cyanide into detergent, or detergent into cyanide).

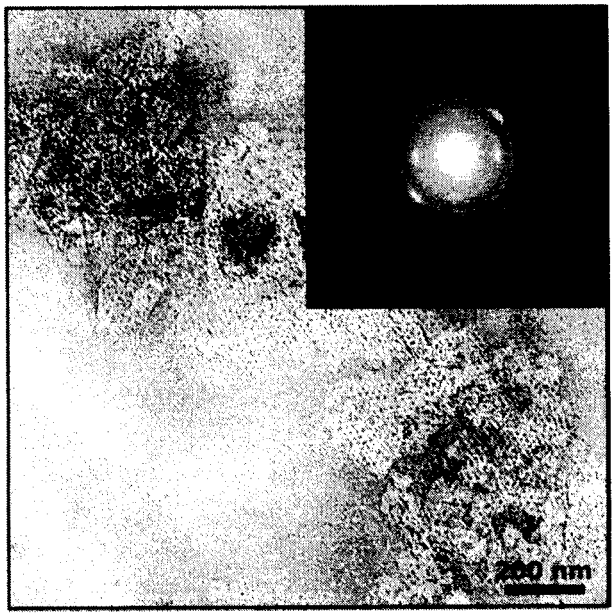

Figure 23: Electrodeposition of gold from a commercial cyanide bath at -800 mV vs. SCE for 5 seconds on AuPd through S-layers of *D. radiodurans*, with corresponding electron diffraction pattern in the inset of a selected region in the patterned area. The spots could not be indexed to elemental gold. The brightest focused ring is a (111) powder diffraction ring corresponding to the AuPd substrate.

It is also conceivable that electroless deposition may proceed by merely immersing the proteins in the bath. The electron source could be provided by dissolved oxygen and all surfaces would act as nucleators to drive a net zero current electrochemical reduction reaction which could still result in seeing the correct electron diffraction patterns. Although generally this process is sped up by adding a reducing agent in the solution, this can still be checked by mimicking the process in the absence of passing current. This is shown in Figure 24 where a parallel electron beam over large regions indicate the lack of any deposits anywhere after long immersion times, and only the structure of the substrate is visible in the diffraction patterns.

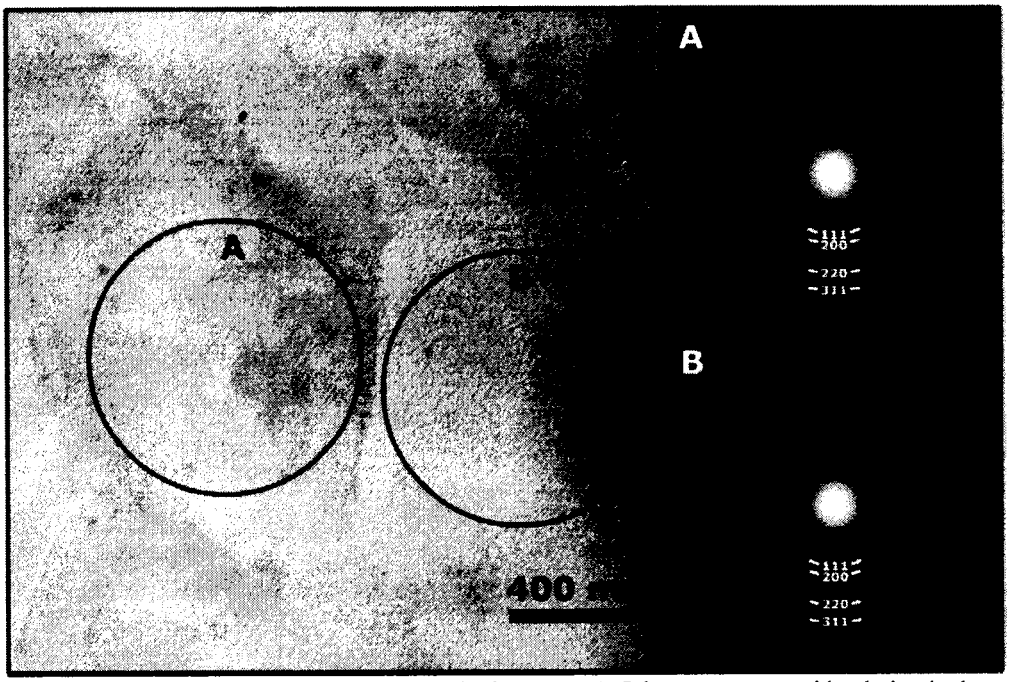

Figure 24: Exposure of S-layers of *D. radiodurans* on AuPd to a cuprous oxide plating bath for 10 minutes without electrodeposition, and corresponding electron diffraction patterns of regions **A)** protein covered area, and **B)** bare area. Marks show positions of simulated diffraction patterns for the AuPd substrate (*i.e.*, face-centered cubic with $a = 0.399$ nm) as usually found in this work.

These summarize the suite of electron diffraction studies typically employed to validate that a material has been successfully electrodeposited through a protein. Additional work not shown is dark field transmission electron microscopy, where a selected crystal orientation is looked at as an image, however, this is ancillary information and used more qualitatively; it could be thought of as performing a bunch of converging beam diffraction experiments simultaneously over a large area.

3.3 Electron Energy-Loss Spectroscopy

3.3.1 Introduction

As previously mentioned in the section on electron diffraction, elemental analysis is useful in cases of failure to identify the failure mode or where the material is not of crystalline nature, or to aid in distinguishing crystal structures where the material is unknown.

In this work, most electron spectroscopy is limited to energy dispersive spectroscopy (EDS) in the SEM on plain films deposited onto bulk substrates to first confirm the electrodeposition, and then confirming the crystal structure by electron diffraction in the transmission electron microscope using the thin metal film substrates. In one case, however, there was an opportunity to exploit facilities at the Pacific Northwest National Laboratory to use the TEM instrument there equipped with an electron energy-loss spectrometer (EELS) system, which affords better localized resolution and does not suffer from the same fluorescence problems encountered with EDS.

3.3.2 Materials and Methods

Preparation of Sample

The sample was that of cuprous oxide electrodeposited through S-layer proteins of *D. radiodurans* prepared as detailed in Chapter 1 in section 1.1.2 under partial coverage conditions as described in Chapter 1 in section 1.2.2 on a self-supported AuPd metal film made as described in Chapter 2 using the methods as described in this chapter in section 3.1.2 at -450 mV vs. SCE for 10 minutes.

Transmission Electron Microscopy and Electron Energy-Loss Spectroscopy (EELS)

EELS was performed on a JEOL 2010 TEM at 200 kV in the Environmental Molecular Sciences Laboratory at Pacific Northwest National Laboratory (PNNL) equipped with a Gatan EELS system. All energy windows are shown with the background subtracted from the spectrum.

3.3.3 Results and Discussion

A sample of cuprous oxide electrodeposited through S-layer proteins of *D. radiodurans* was saved for EELS analysis. Although cuprous oxide had already been confirmed by electron diffraction, it was hoped that other details might be confirmed by EELS, such as whether the presence of protein could be detected, which can not be seen by either imaging (due to the low contrast of carbon) or electron diffraction (due to the lack of "true" crystallinity of the protein). A similar three-phase region containing patterned region, unpatterned region, and bare surface was found for this analysis. The EELS data (with background substracted) is shown in Figure 25.

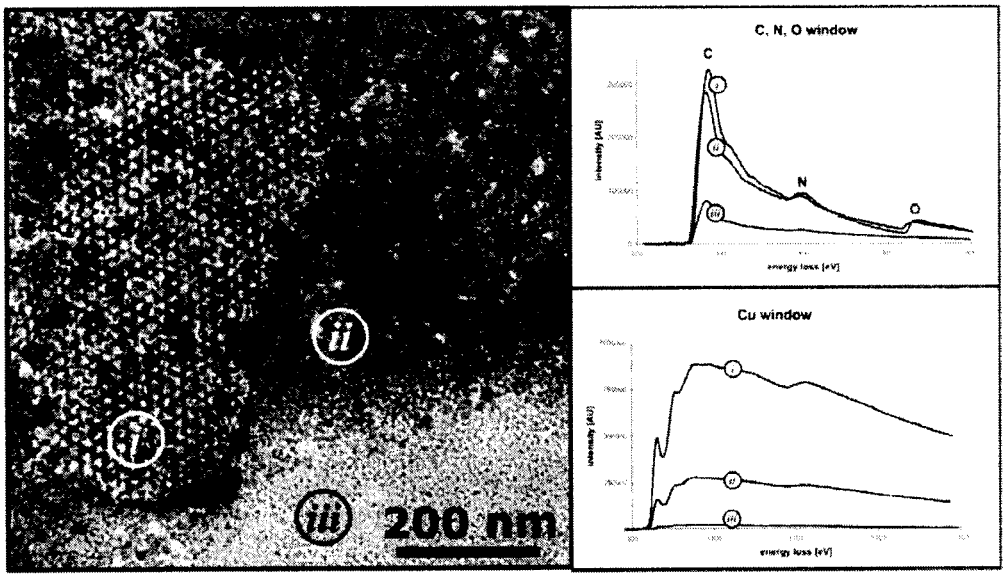

Figure 25: Electron energy-loss spectroscopy of three different kinds of regions: (*i*) a patterned cuprous oxide region, (*ii*) a plain cuprous oxide film region, and (*iii*) the bare surface. Two different energy windows are shown, one window shows carbon, nitrogen, and oxygen energy-loss edges, another shows just the copper edge.

The results shown in Figure 25 were intially quite surprising, in that there is presence of combined carbon, nitrogen, and oxygen on a plain film area. This implies that there is protein present in this region, even though no patterning is apparent there. The reduced signal of copper could be a result of a thicker growth of cuprous oxide (though the oxygen signal should then be anomalous by comparison to nitrogen and carbon), but most likely, there is a protein sheet sitting *on top* of the plain Cu_2O film.

The theory here is that the structure is a bilayer of plain Cu_2O, which is of comparable thickness to that of the structured film, with protein on top of it. This would imply that, when the proteins are submerged in the electrolyte, there is some probability that some portions are not well adhered to the surface and become momentarily freed, though still attached to the portions that are well adhered. Electrodeposition proceeds as normal, and only forms nanostructures where proteins are physically still attached to the surface. After removal from the electrolyte, dangling portions of the protein then may land back on the surface (which is now the freshly deposited surface). The image is overwhelmed by the high contrast of the film to see the proteins directly, and diffraction will not pick them out unless they are truly atomically ordered. However, spectroscopy can detect them if they contain elements not normally seen (such as nitrogen). Had this been thought of at the time, a further experiment to perform would be to continue probing with EELS further away until the nitrogen signal disappears to see how much effect the protein thickness has on the copper signal.

3.4 Three-dimensional reconstruction of the material

3.4.1 Introduction

Though plan-view transmission electron microscopy was an incredible achievement using the platform developed as discussed in Chapter 2, the lack of a full three-dimensional model severely limits what can be discussed in terms of the concept of moulding throughout the protein void space. It is expected that the deposit should be in contact with the surface, and that it shall have filled some, if not most or all, of the internal molecular architecture of the protein up to the height of the deposit. Fortunately, the need for three-dimensional imaging in transmission electron microscopy has been a solved problem and the general strategy involves tilting the sample in the microscope on one or multiple axes and combining the projected views and back-calculating the 3D electron density using known microscope and electron lens parameters. Because this work involves periodic objects the objective was to try the correlation averaging technique [94] to obtain better spatial information. Though this process will undoubtedly eliminate many variations in individual structures, this will provide an average view of where growth is limited, *i.e.*, the deposition envelope.

Only the best quality samples were to be sent to callaborators at the Scripps Institute in La Jolla, CA. Multiple samples were prepared and only those where high-quality regions could be found near the centers of grid windows where high-angle tilting could be performed were sent for study. Samples were prepared of cuprous oxide electrodeposited through S-layers of both *D. radiodurans* and *S. ureae*.

3.4.2 Materials and Methods

Preparation of Samples

The sample was that of cuprous oxide electrodeposited through S-layer proteins of *D. radiodurans* and *S. ureae* prepared as detailed in Chapter 1 in section 1.1.2 under partial coverage conditions as described in Chapter 1 in section 1.2.2 on self-supported Pt metal films made as described in Chapter 2 using the methods as described in this chapter in section 3.1.2 at -450 mV vs. SCE for 15 minutes.

3D reconstruction by TEM

3D reconstructions were performed by Anchi Cheng at the National Resource for Automated Molecular Microscopy, in the Department of Cell Biology at the Scripps Research Institute in La Jolla, CA. Averaging was performed over 5 different patterned regions using dual tilting up to 70° after unbending each image and warping to fit a perfect lattice.

3.4.3 Results and Discussion

The first calculation involves an "unbending" which is required to displace all periodic elements to their least squares positions in a perfect lattice permitting higher quality averaging. This is performed over two orthogonal tilt axes, an example of such a series (in one of the axes) is shown in Figure 26 for the structure formed around *D. radiodurans*.

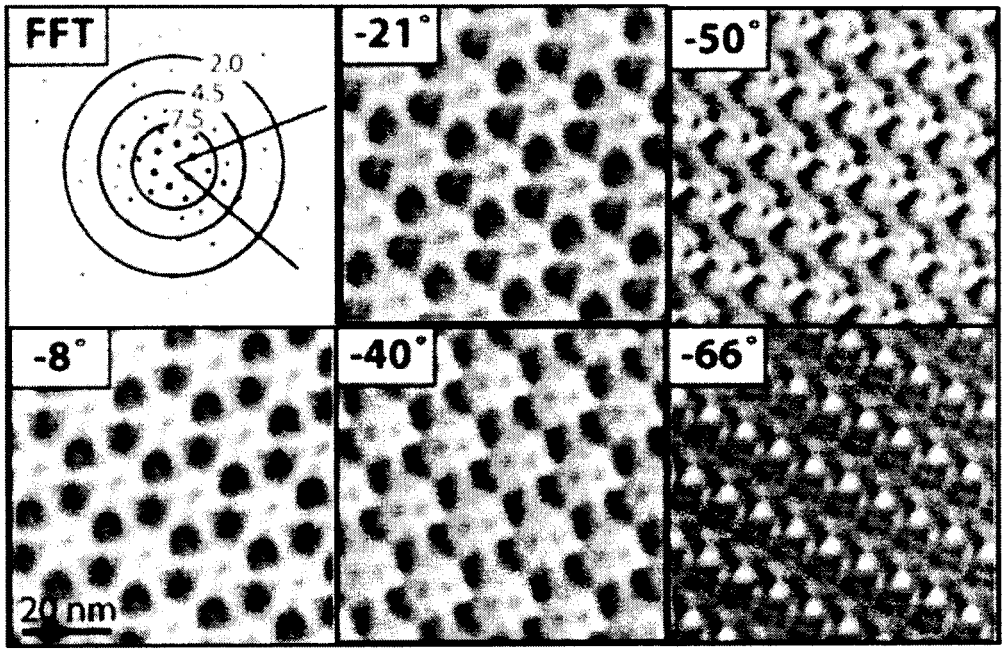

Figure 26: Sample of recorded tilt series along one tilt axis (after unbending) of cuprous oxide electrodeposited through S-layers of *D. radiodurans* at -450 mV vs. SCE for 15 minutes on Pt. FFT shows information out to about 3 – 4 nm.

The images are a result of projection of the electrons passing through a three-dimensional object onto a planar surface, the imaging camera. With automated centering and focusing stages, the two-dimensional projections contain information about the sample in a "negative pyramid" shape, where the missing information is lost due to physical limits on the tilt angle, here 70° as is typical.

In this work, there are two types of periodic objects, an electron light object and an electron dense object. However, the calculations result in numbers which correspond to the electron density in x, y, and z space. Generally, the data is represented in 2D as a series of contours at regular intervals of electron density, or it may be rendered in 3D as a surface-shaded volume if a proper contour can be chosen as the "cut-off" density.

To represent the data, a freely available software package called Chimera is available that permits the rendering of surfaces by choosing the "cut-off" for the electron density contour. For the protein, which is very low in electron density, the choice is very clear because its structure is inwardly shaped, has finite mass, and was previously determined by others. For the inorganic nanostructure, the choice of the cut-off is not as clear, so for representation a "reasonable" cut-off is chosen, one that stops before obvious artifacts are seen, *i.e.*, strange periodic features in the z-direction that appear above and below the plane of the "cube" representing the volume of the unit cell. The finalized data, with various views and cross-sections, is shown in Figure 27.

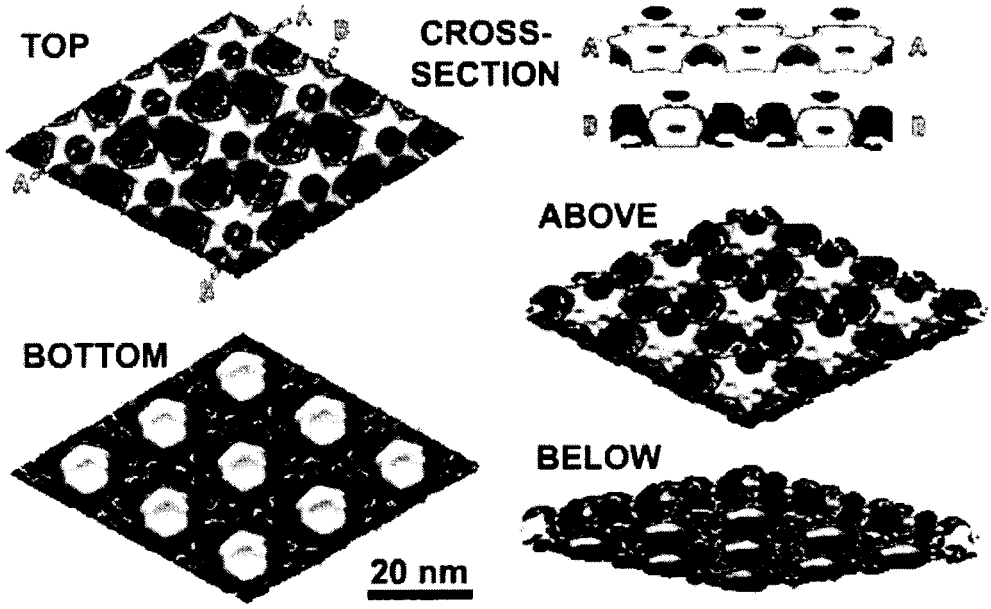

Figure 27: Various views of the 3D reconstruction from cuprous oxide deposit through S-layers of *D. radiodurans*, from top, bottom, tilted, and cross-sections through the six-fold symmetric sites and through the three-fold symmetric sites.

What can be seen in Figure 27 is that material growth is occuring underneath structural features such as the connecting arms and is just about to proceed over and around them, thought at the average thickness of this particular deposit, complete moulding had not yet occurred. Also of interest is that in the finer features the average thickness is taller (look at cross-sections A and B), than in the more open spaces. This is potentially another manifestation of the classical current crowding effect due to field lines, *i.e.*, the Laplacian of the potential field is zero (to a first approximation). A non-mathematical way to think of it is that, just as sharp points make good field emitters, sharp pits make good field absorbers.

Unfortunately, no data is presented for the reconstruction of *S. ureae* templated structures. There was only a very tiny structural feature with scattered fragmentation patterns which were so difficult to interpret that it would be erroneous to report it. Considering how dense the 3D structure of the protein is and how fine the open space is, it is not a surprise considering the best resolution attained was 3 nm.

CONCLUSIONS

The ability to use the imaging platform developed in Chapter 2 to perform transmission electron microscopy and its corresponding capabilities in terms of imaging, diffraction, and spectroscopy, has allowed a very wide view of the nanoscale architecture of electrodeposited material through and around the S-layer proteins of *Deinococcus radiodurans* and *Sporosarcina ureae*. The best data came from *Deinococcus radiodurans* as a result of its larger, more open structure, as well as its incredibly high tolerance to wide variations in acidity. In the case of *Sporosarcina ureae*, only cuprous oxide could be successfully deposited. In terms of 3D structure, we can see the effects of the moulding process clearly around the S-layers of *D. radiodurans*, that connecting structures are surrounded by deposit, that deposit appears to make good contact with the surface (although it is not visible in the reconstruction, it stops suddenly in the same plane as the bottom of the protein), and the average variation in thickness follows from traditional electrodeposition concepts such as crowding of electrical field lines in finer patterns such as the central hole over the larger openings. For *S. ureae*, the 3D reconstruction was of insufficient resolution to see anything but a tiny blob of material and speckles floating in space, despite clearly seeing the pattern in plan-view images.

CLOSING STATEMENTS

Having proven a new method for fabricating nanostructures directly on surfaces, here the chapters are generalized to extract their most useful concepts for those who want to go further.

Chapter 1 discusses how a protein is selected and tested for suitability in a fabrication environment. In general, the protein selection will be one's choice. To prove the concept, obviously only "easy" proteins will be chosen, that is, proteins that can be easily purified from organisms that be can easily maintained and grown. For example, one might not want to bleed rabbits constantly day after day to get micrograms of protein for one experiment. That is why Table 1 is organized by structure, then protein, organism, and reference. There may be a trade-off, how exact does the fabrication have to be, and can you get away with something a little different to save a lot of hassle? These are the questions one should ask at the beginning if one is serious to build something.

In the next section of Chapter 1, a particular protein is selected for a stability study. Here, a pretty wide range of conditions is studied and analyzed. However, this would not need to be done in practice. It would be wise to test the chosen protein under the conditions one intends to operate in, and if it is disrupted, begin moving "outwards" towards more neutral zones in whichever manner desired until a stability edge is found. Quantification is not necessary, one must merely find the envelope.

Chapter 2 is about how a thin metal film platform was developed which allows transmission electron microscopy to be performed on noble metal surfaces, the best surfaces for good electrodeposition work. It is hoped that over time, these will simply be commercially available, but until then, there's Chapter 2 and the Appendix.

Chapter 3 is about how the transmission electron microscope was used to validate the electrodeposition work. Clearly, not all of this work must be repeated under all circumstances. The easiest thing to do, provided one has TEM capabilities, is to perform elemental spectroscopy using an x-ray spectrometer (EDS). As mentioned in the text, this is not ideal nor does it "prove" much, but it is fast and easy to do if one has the detector. If one uses a scanning electron microscope (SEM), one will not easily see these structures, and EDS only tells you about elements.

Finally, the fabrication strategy proven in this work begins the idea of using the combination of proteins and electrochemistry together to build solid-state structures on surfaces. Biological and chemical sensors are the first likely platform for which a fabrication system like this is most readily suited, because the orientation of the sensing component, as well as its size and density are figures of merit. Because the two S-layers used in this work are stabilized by detergents, it is most likely that they have two different sides which may be used to preferentially adsorb one side to a surface. In this work high energy substrates are used for the nucleation densities needed, here the challenge would be for one to find conditions that permit the overwhelming majority of adsorbed S-layers to exposed a certain side for sensitivity.

Another challenge arises due to the lack of atomic resolution information on S-layer proteins, thus making it difficult to genetically fuse an appropriate sensing attachment in an ideal location on the protein surface. Although one might consider using another type of protein, the advantage of S-layers may prove to outweigh the use of other proteins due to the need for overexpression by genetic engineering and the need for recrystallization of the monomeric complexes. For example, without knowing the crystal structure, S-layers of *Bacillus stearothermophilus* have been successfully fused with other proteins and have demonstrated both the ability to organize into ordered arrays as well as maintain the function of the fused protein.[126, 127] There

are also techniques for finding potential insertion sites in proteins without knowing their structures in advance.[128]

The first materials for which one might consider sensing would be that of the protein itself. Because cuprous oxide has demonstrated a high fidelity moulding process, and has strong optical absorption in the blue due to its excitonic properties,[129] a strong surface enhanced Raman effect may potentially be seen for any protein residues coming into intimate contact with cuprous oxide. However, it may be necessary to change the material to observe the effect more pronouncedly. If a certain residue has a unique spectroscopic signature, it may be possible to get a crude map of which residues that are solvent exposed, thus gleaning additional insight into S-layer protein structure which has fascinated biochemists since their discovery in 1953.[130]

WORKS CITED

[1] Ritter, S. K., "Planning nanotech from the ground up," *Chem. & Engr. News*, 84 (2006) 37-40.

[2] Sander, M. S., Prieto, A. L., Gronsky, R., Sands, T., and Stacy, A. M., "Fabrication of high-density, high aspect ratio, large-area bismuth telluride nanowire arrays by electrodeposition into porous anodic alumina templates," *Adv. Mater.*, 14 (2002) 665-7.

[3] Park, M., Harrison, C., Chaikin, P. M., Register, R. A., and Adamson, D. H., "Block copolymer lithography: periodic arrays of ~10^{11} holes in 1 square centimeter," *Science*, 276 (1997) 1401-4.

[4] Sleytr, U. B., Messner, P., Pum, D., and Sára, M., "Crystalline bacterial cell surface layers (S layers): From supramolecular cell structure to biomimetics and nanotechnology," *Angew. Chem. Int. Edit.*, 38 (1999) 1034-54.

[5] Shenton, W., Pum, D., Sleytr, U. B., and Mann, S., "Synthesis of cadmium sulfide superlattices using self-assembled bacterial S-layers," *Nature*, 389 (1997) 585-7.

[6] Mertig, M., Kirsch, R., Pompe, W., and Engelhardt, H., "Fabrication of highly ordered nanocluster arrays by biomolecular templating," *Eur. Phys. J. D*, 9 (1999) 45-8.

[7] Hall, S. R., Shenton, W., Engelhardt, H., and Mann, S., "Site-specific organization of gold nanoparticles by biomolecular templating," *ChemPhysChem*, (2001) 184-6.

[8] McMillan, R. A., Paavola, C. D., Howard, J., Chan, S. L., Zaluzec, N. J., and Trent, J. D., "Ordered nanoparticle arrays formed on engineered chaperonin protein templates," *Nat. Mater.*, 1 (2002) 247-52.

[9] Douglas, K., Devaud, G., and Clark, N. A., "Transfer of biologically derived nanometer-scale patterns to smooth surfaces," *Science*, 257 (1992) 642-4.

[10] Malkinski, L., Camley, R. E., Celinski, Z., Winningham, T. A., Whipple, S. G., and Douglas, K., "Hexagonal lattice of 10-nm magnetic dots," *J. Appl. Phys.*, 93 (2003) 7325-7.

[11] Moore, J. T., Beale, P. D., Winningham, T. A., and Douglas, K., "Creation of nanometer-scale patterns with selected metal films," *Appl. Phys. Lett.*, 72 (1998) 1840-2.

[12] Panhorst, M., Brückl, H., Kiefer, B., Reiss, G., Santarius, U., and Guckenberger, R., "Formation of metallic surface structures by ion etching using a S-layer template," *J. Vac. Sci. Technol. B*, 19 (2001) 722-4.

[13] Winningham, T. A., Whipple, S. G., and Douglas, K., "Pattern transfer from a biomolecular nanomask to a substrate via an intermediate transfer layer," *J. Vac. Sci. Technol. B*, 19 (2001) 1796-802.

[14] Wahl, R., Mertig, M., Raff, J., Selenska-Pobell, S., and Pompe, W., "Electron-beam induced formation of highly ordered palladium and platinum nanoparticle arays on the S Layer of *Bacillus sphaericus* NCTC 9602," *Adv. Mater.*, 13 (2001) 736-40.

[15] Datta, M. and Landolt, D., "Fundamental aspects and applications of electrochemical microfabrication," *Electrochim. Acta*, 45 (2000) 2535-58.

[16] Ekwall, P., Mandell, L., and Fontell, K., "Solubilization in micelles and mesophases and the transition from normal to reverse structures," *Mol. Cryst. Liq. Cryst.*, 8 (1969) 157 - 213.

[17] Thurn-Albrecht, T., Schotter, J., Kästle, G. A., Emley, N., Shibauchi, T., Krusin-Elbaum, L., Guarini, K., Black, C. T., Tuominen, M. T., and Russell, T. P., "Ultrahigh-density nanowire arrays grown in self-assembled diblock copolymer templates," *Science*, 290 (2000) 2126-9.

[18] Peters, J., Peters, M., Lottspeich, F., Schäfer, W., and Baumeister, W., "Nucleotide sequence analysis of the gene encoding the *Deinococcus radiodurans* surface protein, derived amino acid sequence, and complementary protein chemical studies," *J. Bacteriol.*, 169 (1987) 5216-23.

[19] Müller, D. J., Fotiadis, D., Scheuring, S., Müller, S. A., and Engel, A., "Electrostatically balanced subnanometer imaging of biological specimens by atomic force microscope," *Biophys. J.*, 76 (1999) 1101-10.

[20] Hall, C. E., "Electron densitometry of stained virus particles," *J. Biophys. Biochem. Cytol.*, 1 (1945) 1-11.

[21] Williams, R. C. and Wyckoff, R. W. G., "The thickness of electron microscopic objects," *J. Appl. Phys.*, 15 (1944) 712-6.

[22] Murray, R. G. E., in *Advances in Paracrystalline Bacterial Surface Layers*, Beveridge, T. J., and Koval, S. F. (Ed.), vol. 252, Plenum Press (1992) pp 3-9.

[23] Engelhardt, H. and Peters, J., "Structural research on surface layers: A focus on stability, surface layer homology domains, and surface layer–cell wall interactions," *J. Struct. Biol.*, 124 (1998) 276-302.

[24] Hebert, H., Skriver, E., Söderholm, M., and Maunsbach, A. B., "Three-dimensional structure of renal Na,K-ATPase determined from two-dimensional membrane crystals of the p1 form," *J. Ultrastruct. Mol. Struct. Res.*, 100 (1988) 86-93.

[25] Roberts, K., Shaw, P. J., and Hills, G. J., "High-resolution electron microscopy of glycoproteins: the crystalline cell wall of *Lobomonas*," *J. Cell Sci.*, 51 (1981) 295-321.

[26] Sára, M., Pum, D., Küpcü, S., Messner, P., and Sleytr, U. B., "Isolation of two physiologically induced variant strains of *Bacillus stearothermophilus* NRS 2004/3a and characterization of their S-layer lattices," *J. Bacteriol.*, 176 (1994) 848-60.

[27] Pum, D., Sára, M., and Sleytr, U. B., "Structure, surface charge, and self-assembly of the S-layer lattice from *Bacillus coagulans* E38-66," *J. Bacteriol.*, 171 (1989) 5296-303.

[28] Roberts, K., "Crystalline glycoprotein cell walls of algae: Their structure, composition, and assembly," *Phil. Trans. R. Soc. Lond. B*, 268 (1974) 129-46.

[29] Roberts, K. and Hills, G. J., "The crystalline glycoprotein cell wall of the green alga *Chlorogonium elongatum*: A structural analysis," *J. Cell Sci.*, 21 (1976) 59-71.

[30] Marr, K. M., McFeeters, R. L., and Lyon, M. K., "Isolation and structural analysis of two-dimensional crystals of photosystem II from *Hordeum vulgare viridis zb*^{63}," *J. Struct. Biol.*, 117 (1996) 86-98.

[31] Le Faou, A., Rajagopal, B. S., Daniels, L., and Fauque, G., "Thiosulfate, polythionates, and elemental sulfur assimilation and reduction in the bacterial world," *FEMS Microbiol. Rev.*, 75 (1990) 351-82.

[32] Hills, G. J., Gurney-Smith, M., and Roberts, K., "Structure, composition, and morphogenesis of the cell wall of *Chlamydomonas reinhardi*. II. Electron microscopy and optical diffraction analysis," *J. Ultrastruct. Res.*, 43 (1973) 179-92.

[33] Stewart, M., Beveridge, T. J., and Murray, R. G. E., "Structure of the regular surface layer of *Spirillum putridiconchlyum*," *J. Mol. Biol.*, 137 (1980) 1-8.

[34] Smit, E., Oling, F., Demel, R., Martinez, B., and Pouwels, P. H., "The S-layer protein of *Lactobacillus acidophilus* ATCC 4356: identification and characterisation of domains responsible for S-protein assembly and cell wall binding," *J. Mol. Biol.*, 305 (2001) 245-57.

[35] Karrasch, S., Typke, D., Walz, T., Miller, M., Tsiotis, G., and Engel, A., "Highly ordered two-dimensional crystals of photosystem I reaction center from *Synechococcus* sp.: functional and structural analyses," *J. Mol. Biol.*, 262 (1996) 336-48.

[36] T'ang, F.-F., Chang, H.-L., Huang, Y.-T. u., and Wang, K. o.-C. i., "Studies on the etiology of trachoma with special reference to isolation of the virus in check embryo," *Chin. Med. J.*, 75 (1957) 429-47.

[37] Matricardi, V. R., Moretz, R. C., and Parsons, D. F., "Electron diffraction of wet proteins: catalase," *Science*, 177 (1972) 268-70.

[38] Hirai, T., Heymann, J. A. W., Shi, D., Sarker, R., Maloney, P. C., and Subramaniam, S., "Three-dimensional structure of a bacterial oxalate transporter," *Nat. Struct. Biol.*, 9 (2002) 597-600.

[39] Behlau, M., Mills, D. J., Quader, H., Kühlbrandt, W., and Vonck, J., "Projection structure of the monomeric porin OmpG at 6 Å resolution," *J. Mol. Biol.*, 305 (2001) 71-7.

[40] Baldermann, C. and Engelhardt, H., "Expression, two-dimensional crystallization, and three-dimensional reconstruction of the β8 outer membrane protein Omp21 from *Comamonas acidovorans*," *J. Struct. Biol.*, 131 (2000) 96-107.

[41] Ziegler, C., Morbach, S., Schiller, D., Krämer, R., Tziatzios, C., Schubert, D., and Kühlbrandt, W., "Projection structure and oligomeric state of the osmoregulated sodium/glycine betaine symporter BetP of Corynebacterium glutamicum," *J. Mol. Biol.*, 337 (2004) 1137-47.

[42] Parcej, D. N. and Eckhardt-Strelau, L., "Structural characterisation of neuronal voltage-sensitive K^+ channels heterologously expressed in *Pichia pastoris*," *J. Mol. Biol.*, 333 (2003) 103-16.

[43] Wells, B., Horne, R. W., Lund, B. M., and King, N. R., "The ultrastructure of *Pseudomonas avenae* - I. Paracrystalline surface layer and extracellular material," *Micron*, 14 (1983) 11-28.

[44] Dooley, J. S. G., Engelhardt, H., Baumeister, W., Kay, W. W., and Trust, T. J., "Three-dimensional structure of an open form of the surface layer from the fish pathogen *Aeromonas salmonicida*," *J. Bacteriol.*, 171 (1989) 190-7.

[45] Bingle, W. H., Whippey, P. W., Doran, J. L., Murray, R. G. E., and Page, W. J., "Structure of the *Azotobacter vinelandii* surface layer," *J. Bacteriol.*, 169 (1987) 802-10.

[46] Crowther, R. A. and Sleytr, U. B., "An analysis of the fine structure of the surface layers from two strains of *Clostridia*, including corrections for distored images," *J. Ultrastruct. Res.*, 58 (1977) 41-9.

[47] Lepault, J., Martin, N., and Leonard, K., "Three-dimensional structure of the T-layer of *Bacillus sphaericus*," *J. Bacteriol.*, 168 (1986) 303-8.

[48] Al-Karadaghi, S., Wang, D. N., and Hovmöller, S., "Three-dimensional structure of the crystalline surface layer from *Aeromonas hydrophila*," *J. Ultrastruct. Mol. Struct. Res.*, 101 (1988) 92-7.

[49] Finch, J. T., Klug, A., and Nermut, M. V., "The structure of the macromolecular units on the cell walls of *Bacillus polymyxa*," *J. Cell Sci.*, 2 (1967) 587-90.

[50] Chalcroft, J. P., Engelhardt, H., and Baumeister, W., "Three-dimensional structure of a regular surface layer from *Pseudomonas acidovorans*," *Arch. Microbiol.*, 144 (1986) 196-200.

[51] Ellar, D. J. and Lundgren, D. G., "Ordered substructure in the cell wall of *Bacillus cereus*," *J. Bacteriol.*, 94 (1967) 1778-80.

[52] Lapchine, L., "Regularly arranged structures on the surface of some *Pseudomonas* sp.," *FEMS Microbiol. Lett.*, 5 (1979) 223-5.

[53] Hasler, L., Walz, T., Tittmann, P., Gross, H., Kistler, J., and Engel, A., "Purified lens major intrinsic protein (MIP) forms highly ordered tetragonal two-dimensional arrays by reconstitution," *J. Mol. Biol.*, 279 (1998) 855-64.

[54] Stahlberg, H., Fotiadis, D., Scheuringa, S., Rémigy, H., Braun, T., Mitsuoka, K., Fujiyoshi, Y., and Engel, A., "Two-dimensional crystals: a powerful approach to assess structure, function and dynamics of membrane proteins," *FEBS Lett.*, 504 (2001) 166-72.

[55] Mitra, A. K., Yeager, M., van Hoek, A. N., Wiener, M. C., and Verkman, A. S., "Projection structure of the CHIP28 water channel in lipid bilayer membranes at 12-Å resolution," *Biochemistry*, 33 (1994) 12735-40.

[56] Chen, Y., Lu, Y.-J., Wang, H.-W., Quan, S., Chang, Z., and Sui, S.-F., "Two-dimensional crystallization of a small heat shock protein HSP16.3 on lipid layer," *Biochem. Biophys. Res. Commun.*, 310 (2003) 360-6.

[57] Valpuesta, J. M., Carrascosa, J. L., and Henderson, R., "Analysis of electron microscope images and electron diffraction patterns of thin crystals of ϕ29 connectors in ice," *J. Mol. Biol.*, 240 (1994) 281-7.

[58] Walz, T., Typke, D., Smith, B. L., Agre, P., and Engel, A., "Projection map of aquaporin-1 determined by electron crystallography," *Nat. Struct. Biol.*, 2 (1995) 730-2.

[59] Scheuring, S., Ringler, P., Borgnia, M. J., Stahlberg, H., Müller, D. J., Agre, P., and Engel, A., "High resolution AFM topographs of the *Escherichia coli* water channel aquaporin Z," *EMBO J.*, 18 (1999) 4981-7.

[60] Unwin, P. N. T. and Henderson, R., "Molecular structure determination by electron microscopy of unstained crystalline specimens," *J. Mol. Biol.*, 94 (1975) 425-40.

[61] Sleytr, U. B. and Glauert, A. M., "Ultrastructure of the cell walls of two closely related Clostridia that possess different regular arrays of surface subunits," *J. Bacteriol.*, 126 (1976) 869-82.

[62] Kühlbrandt, W., Wang, D. N., and Fujiyoshi, Y., "Atomic model of plant light-harvesting complex by electron crystallography," *Nature*, 367 (1994) 614-21.

[63] Ellis, M. J., Knapp, S., Koeck, P. J. B., Fakoor-Biniaz, Z., Ladenstein, R., and Hebert, H., "Two-dimensional crystallization of the chaperonin TF55 from the hyperthermophilic archaeon *Sulfolobus solfataricus*," *J. Struct. Biol.*, 123 (1998) 30-6.

[64] Dorset, D. A., "Direct phasing in protein electron crystallography - phase extension and the prospects for *ab initio* determinations," *Acta Crystallogr. A*, 52 (1996) 480-9.

[65] Kerosuo, E., Haapasalo, M., Ranta, H., and Lounatmaa, K., "Hexagonal periodicity in the outer membrane of *Bacteroides buccae*," *J. Gen. Microbiol.*, 133 (1987) 2217-24.

[66] Rachel, R., Jakubowski, U., Tietz, H., Hegerl, R., and Baumeister, W., "Projected structure of the surface protein of *Deinococcus radiodurans* determined to 8 Å resolution by cryomicroscopy," *Ultramicroscopy*, 20 (1986) 305-16.

[67] Smit, J., Grano, D. A., Glaeser, R. M., and Agabian, N., "Periodic surface array in *Caulobacter crescentus*: fine structure and chemical analysis," *J. Bacteriol.*, 146 (1981) 1135-50.

[68] Cheong, G.-W., Guckenberger, R., Fuchs, K.-H., Gross, H., and Baumeister, W., "The structure of the surface layer of *Methanoplanus limicola* obtained by a combined electron microscopy and scanning tunneling microscopy approach," *J. Sctruct. Biol.*, 111 (1993) 125-34.

[69] Chang, J.-J., Leonard, K., Arad, T., Pitt, T., Zhang, Y.-X., and Zhang, L.-H., "Structural studies of the outer envelope of *Chlamydia trachomatis* by electron microscopy," *J. Mol. Biol.*, 161 (1982) 579-90.

[70] Austin, J. W., Engel, A., Murray, R. G. E., and Aebi, U., "Structural analysis of the S-layer of *Lampropedia hyalina*," *J. Ultrastruct. Mol. Struct. Res.*, 102 (1989) 255-64.

[71] Rasch, M., Saxton, W. O., and Baumeister, W., "The regular surface layer of *Acetogenium kivui*: Some structural, developmental, and evolutionary aspects," *FEMS Microbiol. Lett.*, 24 (1984) 285-90.

[72] Sleytr, U. B., Sára, M., Küpcü, S., and Messner, P., "Structural and chemical characterization of S-layers of selected strains of *Bacillus stearothermophilus* and *Desulfotomaculum nigrificans*," *Arch. Microbiol.*, 146 (1986) 19-24.

[73] Brock, T. D., Brock, K. M., Belly, R. T., and Weiss, R. L., "Sulfolobus: a new genus of sulfur-oxidizing bacteria living at low pH and high temperature," *Arch. Mikrobiol.*, 84 (1972) 54-68.

[74] Zillig, W., Stetter, K. O., Prangishvilli, D., Schäfer, W., Wunderl, S., Janekovic, D., Holz, I., and Palm, P., "*Desulfurococcaceae*, the second family of the extremely thermophilic, anaerobic, sulfur-respiring *Thermoproteales*," *Zentralbl. Bakteriol. Mikrobiol. Hyg., 1*, C3 (1982) 304-17.

[75] Bradford, M. M., "A rapid and sensitive method for the quantitation of microgram quantities of protein utilizing the principle of protein-dye binding," *Anal. Biochem.*, 72 (1976) 248-54.

[76] Garfin, D. E., "One-dimensional gel electrophoresis," *Methods Enzymol.*, 182 (1990) 425-41.

[77] Oh, J., Tak, Y., and Lee, J., "Electrodeposition of Cu_2O nanowires using nanoporous template," *Electrochem. Solid St.*, 7 (2004) C27-C30.

[78] Messner, P., Hollaus, F., and Sleytr, U. B., "Paracrystalline cell-wall surface-layers of different *Bacillus Stearothermophilus* strains " *Int. J. Syst. Bacteriol.*, 34 (1984) 202-10.

[79] Schäffer, C., Wugeditsch, T., Kählig, H., Scheberl, A., Zayni, S., and Messner, P., "The surface layer (S-layer) glycoprotein of *Geobacillus stearothermophilus* NRS 2004/3a," *J. Biol. Chem.*, 277 (2002) 6230-9.

[80] Egelseer, E. M., Leitner, K., Jarosch, M., Hotzy, C., Zayni, S., Sleytr, U. B., and Sára, M., "The S-layer proteins of two *Bacillus stearothermophilus* wild-type strains are bound via their N-terminal region to a secondary cell wall polymer of identical chemical composition," *J. Bacteriol.*, 180 (1998) 1488-95.

[81] Hills, G. J., Phillips, J. M., Gay, M. R., and Roberts, K., "Self-assembly of a plant cell wall *in vitro*," *J. Mol. Biol.*, 96 (1975) 431-41.

[82] Davies, D. R. and Plaskitt, A., "Genetical and structural analyses of cell-wall formation in *Chlamydomonas reinhardi*," *Genet. Res.*, 17 (1971) 33-43.

[83] Beveridge, T. J. and Murray, R. G. E., "Superficial macromolecular arrays on the cell wall of *Spirillum putridiconchylium*," *J. Bacteriol.*, 119 (1974) 1019-38.

[84] Lembcke, G., Baumeister, W., Beckmann, E., and Zemlin, F., "Cryo-electron microscopy of the surface protein of *Sulfolobus shibatae*," *Ultramicroscopy*, 49 (1993) 397-406.

[85] Grogan, D. W., Palm, P., and Zillig, W., "Isolate B12, which harbours a virus-like element, represents a new species of archaebacterial genus *Sulfolobus*, *Sulfolobus shibatae*, sp. nov.," *Arch. Microbiol.*, 154 (1990) 594-9.

[86] Lembcke, G., Dürr, R., Hegerl, R., and Baumeister, W., "Image analysis and processing of an imperfect two-dimensional crystal: the surface layer of the archaebacterium *Sulfolobus acidocaldarius* re-investigated," *J. Microsc.*, 161 (1991) 263-78.

[87] Baumeister, W., Volker, S., and Santarius, U., "The three-dimensional structure of the surface protein of *Acidianus brierleyi* determined by electron crystallography," *System. Appl. Microbiol.*, 14 (1991) 103-10.

[88] König, H. and Stetter, K. O., "Studies on archaebacterial S-layers," *System. Appl. Microbiol.*, 7 (1986) 300-9.

[89] Kay, W. W., Buckley, J. T., Ishiguro, E. E., Phipps, B. M., Monette, J. P. L., and Trust, T. J., "Purification and disposition of a surface protein associated with virulence of *Aeromonas salmonicida*," *J. Bacteriol.*, 147 (1981) 1077-84.

[90] Wildhaber, I., Santarius, U., and Baumeister, W., "Three-dimensional structure of the surface protein of *Desulfurococcus mobilis*," *J. Bacteriol.*, 169 (1987) 5563-8.

[91] Engelhardt, H., Saxton, W. O., and Baumeister, W., "Three-dimensional structure of the tetragonal surface layer of *Sporosarcina ureae*," *J. Bacteriol.*, 168 (1986) 309-17.

[92] Beveridge, T. J., "Surface arrays on the wall of *Sporosarcina ureae*," *J. Bacteriol.*, 139 (1979) 1039-48.

[93] Thompson, B. G., Murray, R. G. E., and Boyce, J. F., "The association of the surface array and the outer membrane of *Deinococcus radiodurans*," *Can. J. Microbiol.*, 28 (1982) 1081-8.

[94] Saxton, W. O. and Baumeister, W., "The correlation averaging of a regularly arranged bacterial cell envelope protein," *J. Microsc.*, 127 (1982) 127-38.

[95] Lancy, P., Jr. and Murray, R. G. E., "The envelope of *Micrococcus radiodurans*: isolation, purification, and preliminary analysis of the wall layers," *Can. J. Microbiol.*, 24 (1978) 162-76.

[96] Howard, L., Orenstein, N. S., and King, N. W., "Purification on renografin density gradients of *Chlamydia trachomatis* grown in the yolk sac of eggs," *Appl. Microbiol.*, 27 (1974) 102-6.

[97] Zhang, Y.-X., Xianmin, M., Zhang, L.-H., Su, H., and Li, R., "Studies on the ultrastructure of envelope of elementary bodies of *Chlamydia trachomatis*," *Scientia Sinica*, 23 (1980) 1208-15.

[98] Poindexter, J. S., "Selection for nonbuoyant morphological mutants of *Caulobacter crescentus*," *J. Bacteriol.*, 135 (1978) 1141-5.

[99] Kjems, J. and Garrett, R. A., "An intron in the 23S ribosomal RNA gene of the archaebacterium *Desulfurococcus mobilis*," *Nature*, 318 (1985) 675-7.

[100] Kjems, J. and Garrett, R. A., "Novel expression of the ribosomal RNA genes in the extreme thermophile and archaebacterium *Desulfurococcus mobilis*," *EMBO J.*, 6 (1987) 3521-30.

[101] Kjems, J., Garrett, R. A., and Ansorge, W., "The sequence of the 16S RNA gene and its flanking region from the archaebacterium *Desulfurococcus mobilis*," *System. Appl. Microbiol.*, 9 (1987) 22-8.

[102] Leffers, H., Kjems, J., Østergaard, L., Larsen, N., and Garrett, R. A., "Evolutionary relationships amongst archaebacteria - a comparative study of 23S ribosomal RNAs of a sulphur-dependent extreme thermophile, an extreme halophile, and a thermophilic methanogen," *J. Mol. Biol.*, 195 (1987) 43-61.

[103] Kjems, J. and Garrett, R. A., "Novel splicing mechanism for the ribosomal RNA intron in the archaebacterium *Desulfurococcus mobilis*," *Cell*, 54 (1988) 693-703.

[104] Kjems, J., Jensen, J., Olesen, T., and Garrett, R. A., "Comparison of transfer RNA and ribosomal RNA intron splicing in the extreme thermophile and archaebacterium *Desulfurococcus mobilis*," *Can. J. Microbiol.*, 35 (1989) 210-4.

[105] Fauque, G., LeGall, J., and Barton, L. L., in *Variations in Autotrophic Life*, Shively, J. M., and Barton, L. L. (Ed.), Academic Press (1991) pp 271-337.

[106] Hedderich, R., Klimmek, O., Kröger, A., Dirmeier, R., Keller, M., and Stetter, K. O., "Anaerobic respiration with elemental sulfur and with disulfides," *FEMS Microbiol. Rev.*, 22 (1999) 353-81.

[107] Liesack, W. and Finster, K., "Phylogenetic analysis of five strains of Gram-negative, obligately anaerobic, sulfur-reducing bacteria and description of *Desulfuromusa* gen. nov., including *Desulfuromusa kysingii* sp. nov., *Desulfuromusa bakii* sp. nov., and *Desulfuromusa succinoxidans* sp. nov.," *Int. J. Syst. Bacteriol.*, 44 (1994) 753-8.

[108] Schauder, R. and Kröger, A., "Bacterial sulphur respiration," *Arch. Microbiol.*, 159 (1993) 491-7.

[109] Zillig, W., Holz, I., Janekovic, D., Klenk, H.-P., Imsel, E., Trent, J., Wunderl, S., Forjaz, V. H., Coutinho, R., and Ferreira, T., "*Hyperthermus butylicus*, a hyperthermophilic sulfur-reducing archaebacterium that ferments peptides," *J. Bacteriol.*, 172 (1990) 3959-65.

[110] Baumeister, W., Karrenberg, F., Rachel, R., Engel, A., Ten Heggeler, B., and Saxton, W. O., "The major cell envelope protein of *Micrococcus radiodurans* (R1)," *Eur. J. Biochem.*, 125 (1982) 535-44.

[111] Thompson, B. G. and Murray, R. G. E., "Isolation and characterization of the plasma membrane and the outer membrane of *Deinococcus radiodurans* strain Sark," *Can. J. Microbiol.*, 27 (1981) 729-34.

[112] Emde-Kamola, B. and Karrenberg, F., "Outer membrane-bound protease of *Deinococcus radiodurans*," *FEMS Microbiol. Lett.*, 42 (1987) 69-74.

[113] Madsen, L. D., Weaver, L., and Jacobsen, S. N., "Influence of material properties on TEM specimen preparation of thin films," *Microsc. Res. Techniq.*, 36 (1997) 354-61.

[114] Hamilton, J. F. and Logel, P. C., "Nucleation and growth of Ag and Pd on amorphous carbon by vapor deposition," *Thin Solid Films*, 16 (1973) 49-63.

[115] Carpenter, F. E. and Curcio, J. A., "Preparation of unbacked metallic films," *Rev. Sci. Instrum.*, 21 (1950) 675.

[116] Egelhoff, W. F., Jr. and Tibbetts, G. G., "Growth of copper, nickel, and palladium films on graphite and amorphous carbon," *Phys. Rev. B*, 19 (1979) 5028-35.

[117] Imbusch, A., "Method for preparing thin self-supporting Pb films," *Rev. Sci. Instrum.*, 38 (1967) 974-5.

[118] Poppa, H., Moorhead, D., and Heinemann, K., "Preparation and analysis of particulate metal deposits," *Thin Solid Films*, 128 (1985) 251-67.

[119] Wassermann, E. F. and Hines, R. L., "Growth of thin gold films on rocksalt from 80°K to 475°K," *J. Appl. Phys.*, 38 (1967) 196-201.

[120] Kuehner, A. L., "New tough films and bubbles," *J. Chem. Ed.*, 25 (1948) 211-2.

[121] Weisenberger, L. M. and Burkin, B. J., *Copper plating.* ASM International: 1992; Vol. 5, Surface Engineering, p 167-76.

[122] Stareck, J. E., US Patent #2,081,121 (1937).

[123] Andricacos, P. C., Uzoh, C., Dukovic, J. O., Horkans, J., and Deligianni, H., "Damascene copper electroplating for chip interconnections," *IBM J. Res. Dev.*, 42 (1998) 567-74.

[124] Weisenberger, L. M. and Burkin, B. J., in *ASM Handbook*, (Ed.), vol. 5, Surface Engineering, ASM International (1992) pp 201-12.

[125] Suzaki, A. and Watanabe, T., "Structure of cobalt film electrodeposited from water and five organic solvents," *J. Japan Inst. Metals*, 64 (2000) 869-77.

[126] Breitwieser, A., Egelseer, E. M., Moll, D., Ilk, N., Hotzy, C., Bohle, B., Ebner, C., Sleytr, U. B., and Sára, M., "A recombinant bacterial cell surface (S-layer)-major birch pollen allergen-fusion protein (rSbsC/Ber v1) maintains the ability to self-assemble into regularly structured monomolecular lattices and the functionality of the allergen.," *Protein Eng.*, 15 (2002) 243-9.

[127] Moll, D., Huber, C., Schlegel, B., Pum, D., Sleytr, U. B., and Sára, M., "S-layer-streptavidin fusion proteins as template for nanopatterned molecular arrays," *Proc. Natl. Acad. Sci. USA.*, 99 (2002) 14646-51.

[128] Nelson, B. D., Manoil, C., and Traxler, B., "Insertion mutagenesis of the *lac* repressor and its implications for structure-function analysis," *J. Bacteriol.*, 179 (1997) 3721-8.

[129] Yu, P. Y., Shen, Y. R., and Petroff, Y., "Resonance Raman scattering in Cu_2O at the blue and indigo excitons," *Solid State Commun.*, 12 (1973) 973-5.

[130] Houwink, A. L., "A macromolecular mono-layer in the cell wall of *Spirillum* species," *Biochim. Biophys. Acta*, 10 (1953) 360-6.

BIBLIOGRAPHY

In addition to cited works, the following works were consulted for this dissertation:

Books:

Bard, A. J. and Faulkner, L. R., "Electrochemical Methods: Fundamentals and Applications," 2nd Edition, (John Wiley & Sons, Inc., New York), 2001.

Caiger-Smith, A., "Lustre Pottery: Technique, Tradition and Innovation in Islam and the Western World," (Faber and Faber, London), 1985.

Cao, G., "Nanostructures and Nanomaterials: Synthesis, Properties and Applications," (Imperial College Press, London), 2004.

Deitel, H. M., Deitel, P. J., Courtemarche, C. J., Hamm, J, C., Liperi, J. P., Nieto, T. R., and Yaeger, C.H., "Visual C++.NET: A Managed Code Approach for Experienced Programmers," (Prentice Hall, Upper Saddle River, New Jersey), 2003.

Frankel, F. and Whitesides, G. M., "On the Surface of Things," (Chronicle Books, San Francisco), 1997.

Frankel, F., "Envisioning Science: The Design and Craft of the Science Image," (The MIT Press, Cambridge, Massachusetts), 2002.

Gamma, E., Helm, R., Johnson, R., and Vlissides, J., "Design Patterns: Elements of Reusable Object-Oriented Software," (Addison-Wesley, Boston), 1995.

Glick, B. R. and Pasternack, J. J., "Molecular Biotechnology: Principles and Applications of Recombinant DNA," 2nd Edition, (ASM Press, Wasington D.C.), 1998.

Lide, David R. (ed.), "Handbook of Chemistry and Physics," 79th Edition, (CRC Press, Boca Raton, Florida), 1998.

Plummer, J.D., Deal, M. D., and Griffin, P. B., "Silicon VLSI Technology: Fundamentals, Practice, and Modeling," (Prentice Hall, Upper Saddle River, New Jersey), 2000.

Press, W. H., Flannery, B. P., Teukolsky, S. A., and Vetterling, W. T., "Numerical Recipes: The Art of Scientific Computing," (Cambridge University Press, Cambridge), 1986.

Schlesinger, M. and Paunovic, M. (Eds.), "Modern Electroplating," 4th Edition, (John Wiley & Sons, Inc., New York), 2000.

Sharp, J. and Jagger, J., "Microsoft Visual C#.NET Step by Step: Version 2003," (Microsoft Press, Redmond, Washington), 2003.

Thomson, J. J., "Rays of Positive Electricity and Their Application to Chemical Analyses," (Longmons, Green and Co., London), 1913.

Articles:

Anderson, A. W., Nordon, H. C., Cain, R. F., Parrish, G., and Duggon, D., "Studies on a radio-resistant micrococcus. I. Isolation, morphology, cultural characteristics, and resistance to gamma radiation," *Food Technol.*, 10 (1956) 575-8.

Arakawa, H., Umemura, K., and Ikai, A., "Protein images obtained by STM, AFM and TEM," *Nature*, 258 (1992) 171-3.

Aoyama, K., Ogawa, K., Kimura, Y., and Fujiyoshi, Y., "A method for 2D crystallization of soluble proteins at liquid-liquid interface," *Ultramicroscopy*, 57 (1995) 345-54.

Baneyx, F., "Recombinant protein expression in *Escherichia coli*," *Curr. Opin. Biotech.*, 10 (1999) 411-21.

Bartlett, P. N. and Whitaker, R. G., "Strategies for the development of amperometric enzyme electrodes," *Biosensors*, 3 (1988) 359-79.

Baumgärtner, M. E. and Raub, C. J., "The electrodeposition of platinum and platinum alloys," *Platinum Metals Rev.*, 32 (1988) 188-97.

Bodea, S., Ballou, R., Pontonnier, L., and Molho, P., "Electrochemical growth of iron and cobalt arborescences under a magnetic field: A TEM study," *Phys. Rev. B*, 66 (2002) 224104.

Brooks, B. W. and Murray, R. G. E., "Nomenclature for '*Micrococcus radiodurans*' and other radiation-resistant cocci: *Deinococcaceae* fam. nov. and *Deinococcus* gen. nov., including five species," *Int. J. Syst. Bacteriol.*, 31 (1981) 353-60.

Buttry, D. A. and Ward, M. D., "Measurement of interfacial processes at electrode surfaces with the electrochemical quartz crystal microbalance," *Chem. Rev.*, 92 (1992) 1355-79.

Cha, J. N., Shimizu, K., Zhou, Y., Christiansen, S. C., Chmelka, B. F., Stucky, G. D., and Morse, D. E., "Silicatein filaments and subunits from a marine sponge direct the polymerization of silica and silicones *in vitro*," *Proc. Natl. Acad. Sci. U.S.A.*, 96 (1999) 361-5.

Chabala, J. M., Abboud, F., Dean, R., Weaver, S., Cole, D., Sauer, C., Raymond, F., III, and Hofmann, U., "Lithographic analysis of multipass gray writing strategy for electron-beam pattern generation," *Proc. SPIE*, 3997 (2000) 309-25.

Chan, W. F. and K., O. T. D., "Isolation of *Deinococcus* species from commercial oyster extract," *Appl. Environ. Microbiol.*, 65 (1999) 846-8.

Chen, Y. and Pépin, A., "Nanofabrication: Conventional and nonconventional methods," *Electrophoresis*, 22 (2001) 187-207.

Chung, J., Lee, K.-H., Lee, J., and Ruoff, R. S., "Toward large-scale integration of carbon nanotubes," *Langmuir*, 20 (2004) 3011-7.

Cosnier, S., "Biosensors based on electropolymerized films - new trends," *Anal. Bioanal. Chem.*, 377 (2003) 507-20.

Cotton, J. B. and Scholes, I. R., "Benzotriazole and related compounds as corrosion inhibitors for copper," *Brit. Corros. J.*, 2 (1967) 1-5.

Cowley, J. M. and Rees, A. L. G., "Fourier methods in structure analysis by electron diffraction," *Rep. Prog. Phys.*, 21 (1958) 165-225.

Dancis, A., Yuan, D. S., Haile, D., Askwith, C., Eide, D., Moehle, C., Kaplan, J., and Klausner, R. D., "Molecular characterization of a copper transport protein in *S. cerevisiae*: An unexpected role for copper in iron transport," *Cell*, 76 (1994) 393-402.

Duggan, D. E., Anderson, A. W., Elliker, P. R., and Cain, R. F., "Ultraviolet exposure studies on a gamma radiation resistant micrococcus isolated from food," *Food Res.*, 24 (1959) 376-82.

Dzyaloshinskii, I. E., Lifshitz, E. M., and Pitaevskii, L. P., "The general theory of van der Waals forces," *Adv. Phys.*, 10 (1959) 165-209.

Edwards, M., Hidmi, L., and Gladwell, D., "Phosphate inhibition of soluble copper corrosion by-product release," *Corros. Sci.*, 44 (2002) 1057-71.

El-Tayeb, S. M. and Abed, K. F., "The effects of certain nutritional additives on the activity of *Sporosarcina ureae* in biodegrading oil in the Arabian Gulf water," *Arab Gulf J. Sci. Res.*, 17 (1999) 303-12.

Evans, S. A. G., Elliott, J. M., Andrews, L. M., Bartlett, P. N., Doyle, P. J., and Denuault, G., "Detection of hydrogen peroxide at mesoporous platinum microelectrodes," *Anal. Chem.*, 74 (2002) 1322-6.

Fernández, L. A. and Berenguer, J., "Secretion and assembly of regular surface structures in gram-negative bacteria," *FEMS Microbiol. Rev.*, 24 (2000) 21-44.

Garnett, J. C. M., "Colours in metal glasses, in metallic films, and in metallic solutions – II," *Philos. Trans. R. Soc. Lond., Ser. A, Math. Phys. Sci.*, 203 (1904) 385-420.

Goldman, M. and Wilson, D. A., "Growth of *Sporosarcina ureae* in defined media," *FEMS Microbiol. Lett.*, 2 (1977) 113-5.

Gosline, J. M., DeMont, M. E., and Denny, M. W., "The structure and properties of spider silk," *Endeavour*, 10 (1986) 37-43.

Gray, J. J., "The interaction of proteins with solid surfaces," *Curr. Opin. Struct. Biol.*, 14 (2004) 110-5.

Green, T. A., Liew, M.-J., and Roy, S., "Electrodeposition of gold from a thiosulfate-sulfite bath for microelectronic applications," *J. Electrochem. Soc.*, 150 (2003) C104-10.

Grove, W. R., "On the electro-chemical polarity of gases," *Phil. Trans.*, 142 (1852) 87-101.

Hadian, S. E. and Gabe, D. R., "Developments in platinum electroplating: P & Q salt solution optimization," *Plating Surf. Finish.*, 88 (2001) 93-8.

Handrea, M., Sahre, M., Neubaue, A., Sleytr, U. B., and Kautek, W., "Electrochemistry of nano-scale bacterial surface protein layers on gold," *Bioelectrochemistry*, 61 (2003) 1-8.

Hansen, W. N. and Kolb, D. M., "The work function of emersed electrodes," *J. Electroanal. Chem.*, 100 (1979) 493-500.

Houwink, A. L., "A macromolecular mono-layer in the cell wall of *Spirillum* species," *Biochim. Biophys. Acta*, 10 (1953) 360-6.

Jap, B. K., Zulauf, M., Scheybani, T., Hefti, A., Baumeister, W., Aebi, U., and Engel, A., "2D crystallization - from art to science," *Ultramicroscopy*, 46 (1992) 45-84.

Jerkiewicz, G., Vatankhah, G., Lessard, J., Soriaga, M. P., and Park, Y.-S., "Surface-oxide growth at platinum electrodes in aqueous H_2SO_4. Reexamination of its mechanism through combined cyclic-voltammetry, electrochemical quartz-crystal nanobalance, and Auger electron spectroscopy measurements," *Electrochim. Acta*, 49 (2004) 1451-9.

Jiang, C., Markutsya, S., and Tsukruk, V. V., "Collective and individual plasmon resonances in nanoparticle films obtained by spin-assisted layer-by-layer assembly," *Langmuir*, 20 (2004) 882-90.

Karlin, S. and Mrázek, J., "Predicted highly expressed and putative alien genes of *Deinococcus radiodurans* and implications for resistance to ionizing radiation damage," *Proc. Natl. Acad. Sci. U.S.A.*, 98 (2001) 5240-5.

Kautek, W., Sahre, M., and Soares, D. M., "*In-situ* monitoring of electrochemical double layer structure changes at gold with a phase-controlled quartz microbalance," *Ber. Bunsenges. Phys. Chem.*, 99 (1995) 667-76.

Kellenberger, E., Häner, M., and Wurtz, M., "The wrapping phenomenon in air-dried and negatively stained preparations," *Ultramicroscopy*, 9 (1982) 139-50.

Kelner, M. J., Bagnell, R., Hale, B., and Alexander, N. M., "Inactivation of intracellular copper-zinc superoxide dismutase by copper chelating agents without glutathione depletion and methemoglobin formation," *Free Radic. Biol. Med.*, 6 (1989) 355-60.

Kocur, M. and Martinec, T., "The taxonomic status of *Sporosarcina ureae* (Beijerinck) Orla-Jensen," *Int. Bull. Bacteriol. Nomencl. Taxon.*, 13 (1963) 201-9.

Kolb, D. M., Engelman, G. E., and Ziegler, J. C., "On the unusual electrochemical stability of nanofabricated copper clusters," *Angew. Chem. Int. Ed.*, 39 (2002) 1123-5.

Kolb, D. M., Ullmann, R., and Ziegler, J. C., "Electrochemical nanostructuring," *Electrochim. Acta*, 43 (1998) 2751-60.

Langmuir, I., "The constitution and fundamental properties of solids and liquids. Part I. Solids," *J. Am. Chem. Soc.*, 38 (1916) 2221-95.

Lee, L.-T., Leite, C. A. P., and Galembeck, F., "Controlled nanoparticle assembly by dewetting of charged polymer solutions," *Langmuir*, 20 (2004) 4430-5.

Lin, A. C. and Goh. M. C., "A novel sample holder allowing atomic force microscopy on transmission electron microscopy specimen grids: Repetitive, direct correlation between AFM and TEM images," *J. Microsc. Oxf.*, 205 (2002) 205-8.

Lowry, O. H., Rosebrough, N. J., Farr, A. L., and Randall, R. J., "Protein measurement using the Folin phenol reagent," *J. Biol. Chem.*, 193 (1951) 265-75.

Lu, H. M. and Jiang, Q., "Size-dependent surface energies of nanocrystals," *J. Phys. Chem. B*, 108 (2004) 5617-9.

Lyubinetsky, I., Thevuthasan, S., McCready, D. E., and Baer, D. R., "Formation of single-phase oxide nanoclusters: Cu_2O on $SrTiO_3(100)$," *J. Appl. Phys.*, 94 (2003) 7926-8.

Madden, J. D. and Hunter, I. W., "Three-dimensional microfabrication by localized electrochemical deposition," *J. Microelectromech. S.*, 5 (1996) 24-32.

Mahalingam, T., Chitra, J. S. P., Ravi, G., Chu, J. P., and Sebastian, P. J., "Characterization of pulse plated Cu_2O thin films," 168 (2003) 111-4.

Minne, S. C., Adams, J. D., Yaralioglu, G., Manalis, S. R., Atalar, A., and Quate, C. F., "Centimeter scale atomic force microscope imaging and lithography," *Appl. Phys. Lett.*, 73 (1998) 1742-4.

Moll, D., Huber, C., Schlegel, B., Pum, D., Sleytr, U. B., and Sára, M., "S-layer-streptavidin fusion proteins as template for nanopatterned molecular arrays," *Proc. Natl. Acad. Sci. USA.*, 99 (2002) 14646-51.

Morkved, T. L., Lopes, W. A., Hahm, J., Sibener, S. J., and Jaeger, H. M., "Silicon nitride membrane substrates for the investigation of local structure in polymer thin films," *Polymer*, 39 (1998) 3871-5.

Mukkamala, S. B. and Powell, A. K., "Biomimetic assembly of calcite microtrumpets: crystal tectonics in action," *Chem. Commun.*, (2004) 918-9.

Nomura, T. and Minemura, A., "Behavior of a piezoelectric quartz crystal in an aqueous solution and the application to the determination of minute amount of cyanide," *Nippon Kagaku Kaishi*, 8 (1980) 1621-5.

O'Brien, J. L., Schofield, S. R., Simmons, M. Y., Clark, R. G., Dzurak, A. S., Curson, N. J., Kane, B. E., McAlpine, N. S., Hawley, M. E., and Brown, G. W., "Scanning tunneling microscope fabrication of arrays of phosphorus atom qubits for a silicon quantum computer," *Smart Mater. Struct.*, 11 (2002) 741-8.

Ono, H., Nagae, K., Shimada, Y., Maehara, H., Yagi, T., Muraki, M., and Okunuki, M., "Fabrication of an electrostatic lens array with separate electrodes and shield membranes using the UV-LIGA process," *Sensor. Actuat. A-Phys.*, 97-98 (2002) 416-21.

Padovani, S., Sada, C., Mazzoldi, P., Brunetti, B. G., Borgia, I., Sgamellotti, A., Giulivi, A., D'Acapito, F., and Battaglin, G., "Copper in glazes of Renaissance luster pottery: nanoparticles, ions, and local environment," *J. Appl. Phys.*, 93 (2003) 10058-63.

Pearce-Percy, H., Abboud, F., Garcia, R., and Mankos, M., "Optimization of field-emission columns for next-generation MEBES® systems," *J. Vac. Sci. Technol. B*, 15 (1997) 2754-9.

Permyakov, E. A., Morozov, L. A., Kalinichenko, L. P., and Derezhkov, V. Y., "Interaction of α-lactalbumin with Cu^{2+}," *Biophys. Chem.*, 32 (1988) 37-42.

Petrii, O. A. and Tsirlina, G. A., "Size effects in electrochemistry," *Russ. Chem. Rev.*, 70 (2001) 285-98.

Philipse, A. P. and Maas, D., "Magnetic colloids from magnetotactic bacteria: chain formation and colloidal stability," *Langmuir*, 18 (2002) 9977-84.

Polzot, P., Laruelle, S., Grugeon, S., Dupont, L., and Tarascon, J.-M., "Nano-sized transition metal oxides as negative-electrode materials for lithium-ion batteries," *Nature*, 407 (2000) 496-9.

Rakhshani, A. E. and Varghese, J., "Potentiostatic electrodeposition of cuprous oxide," 157 (1988) 87-95.

Ramanujam, V. V. and Krishnan, U., "Studies on mixed ligand complexes of copper. Part III. Copper-lactate-aminocarboxylate complexes," *J. Indian Chem. Soc.*, 57 (1980) 359-62.

Richter, J., "Metallization of DNA," *Physica E*, 16 (2003) 157-73.

Sarikaya, M., Tamerler, C., Jen, A. K.-Y., Schulten, K., Baneyx, F., "Molecular biomimetics: nanotechnology through biology," *Nat. Mater.*, 2 (2003) 577-85.

Sarikaya, M., Tamerler, C., Schwartz, D. T., Baneyx, F., "Materials assembly and formation using engineered polypeptides," *Annu. Rev. Mat. Res.*, 34 (2004) 373-408.

Schwartz, D. T. and Muller, R. H., "Oxidation films on copper in alkaline media: intensity modulated photoelectrochemical and Raman spectroscopy studies," *Surf. Sci.*, 248 (1991) 349-58.

Shedd, G. M. and Russell, P. E., "The scanning tunneling microscope as a tool for nanofabrication," *Nanotechnology*, 1 (1990) 67-80.

Shipway, A. N., Katz, E., and Willner, I., "Nanoparticle arrays on surfaces for electronic, optical, and sensor applications," *ChemPhysChem*, 1 (2000) 18-52.

Smith, D. R., "Copper 1995," *Coordin. Chem. Rev.*, 164 (1997) 575-666.

Smith, P. K., Krohn, R. I., Hermanson, G. T., Mallia, A. K., Gartner, F. H., Provenzano, M. D., Fujimoto, E. K., Goeke, N. M., Olson, B. J., and Klenk, D. C., "Measurement of protein using bicinchoninic acid," *Anal. Biochem.*, 150 (1985) 76-85.

Southam, G., Fyfe, W. S., and Beveridge, T. J., "Immobilization of free ionic gold and L-asparagine complexed ionic gold by *Sporosarcina ureae*: The importance of organo-gold complexes in gold mobility," *Miner. Metall. Process* . 17 (2000) 129-32.

Spence, J. C. H., "The future of atomic resolution electron microscopy for materials science," *Mater. Sci. Eng. R*, 26 (1999) 1-49.

Stoll, V. S. and Blanchard, J. S., "Buffers: Principles and practice," *Methods Enzymol.*, 182 (1990) 24-38.

Suarez, D. F. and Olson, F. A., "Nodulation of electrodeposited copper in the presence of thiourea," *J. Appl. Electrochem.*, 22 (1992) 1002-10.

Switzer, J. A., Hung, C.-J., Huang, L.-Y., Miller, S., Zhou, Y., Raub, E. R., Shumsky, M. G., and Bohannan, E. W., "Potential oscillations during the electrochemical self-assembly of copper/cuprous oxide layered nanostructures," 13 (1998) 909-16.

Tench, D. and Warren, L. F., "Electrodeposition of conduction transition metal oxide / hydroxide films from aqueous solution," 130 (1983) 869-72.

Van Borm, W. A. and Adams, F. C., "A standardless ZAF correction for semi-quantitative electron probe microanalysis of microscopical particles," *X-ray Spectrom.*, 20 (1991) 51-62.

Vettiger, P., Cross, G., Despont, M., Drechsler, U., Dürig, U., Gotsmann, B., Häberle, W., Lantz, M. A., Rothuizen, H. E., Stutz, R., and Binnig, G. K., "The 'Millipede'—nanotechnology entering data storage," *IEEE Trans. Nanotechnol.*, 1 (2002) 39-55.

Vitos, L., Ruban, A. V., Skriver, H. L., and Kollár, J., "The surface energy of metals," *Surf. Sci.*, 411 (1998) 186-202.

Völkel, D., Zimmermann, K., Breitwieser, A., Pable, S., Glatzel, M., Scheiflinger, F., Schwarz, H. P., Sára, M., Sleytr, U. B., and Dorner, F., "Immunochemical detection of prion protein on dipsticks prepared with crystalline bacterial cell-surface layers," *Transfusion*, 43 (2003).

Wan, R. Y. and Miller, J. D., "Solvation extraction and electrodeposition of gold from cyanide solutions." *J. Metals*, 38 (1986) 35-40.

Wetlaufer, D. B., "Ultraviolet spectra of proteins and amino acids," *Adv. Protein Chem.*, 17 (1962) 303-90.

Whitesides, G. M. and Boncheva, M., "Beyond molecules: self-assembly of mesoscopic and macroscopic components," *Proc. Natl. Acad. Sci. U.S.A.*, 99 (2002) 4769-74.

Williamson, M. J., Tromp, R. M., Vereecken, P. M., Hull, R., and Ross, F. M., "Dynamic microscopy of nanoscale cluster growth at the solid-liquid interface," *Nat. Mater.*, 2 (2003) 532-6.

Wood, O. R., II, Trybula, W. J., Greschner, J., Kalt, S., Bayer, T., Shimizu, S., Yamamoto, H., Suzuki, K., Gordon, M. S., Robinson, C. F., Dhaliwal, R. S., Thiel, C. W., Caldwell, N., Lawliss, M. S., and Huang, C., "Ultrathin membrane masks for electron projection lithography," *J. Vac. Sci. Technol. B*, 22 (2004) 3072-6.

Wu, H.-Q., Wei, X.-W., Shao, M.-W., Gu, J.-S., and Qu, M.-Z., "Synthesis of copper oxide nanoparticles using carbon nanotubes as templates," *Chem. Phys. Lett.*, 364 (2002) 152-6.

Xia, Y. and Whitesides, G. M., "Soft lithography," *Angew. Chem. Int. Ed.*, 37 (1998) 550-75.

Yu, P. Y., Shen, Y. R., and Petroff, Y., "Resonance Raman scattering in Cu_2O at the blue and indigo excitons," *Solid State Commun.*, 12 (1973) 973-5.

Zhou, Y. and Switzer, J. A., "Electrochemical deposition and microstructure of copper (I) oxide films," *Script. Mater.*, 38 (1998) 1731-8.

Zonnevylle, M. C. and Hoffman, R., "The adsorption of benzotriazole on copper and cuprous oxide," *J. Vac. Sci. Technol. A*, 6 (1988) 885-6.

Zoval, J. V., Lee, J., Gorer, S., and Penner, R. M., "Electrochemical preparation of platinum nanocrystallites with size selectivity on basal plane oriented graphite surfaces," *J. Phys. Chem. B*, 102 (1998) 1166-75.

APPENDIX

Additional Works on Thin Metallic Films

The purpose of this appendix is to provide more data on the thin metal film development as well as applications attempted that did not have direct correspondence to the work in the main text. Some of this data is intended for publication, and some is presented because it is believed to be of some use but not of sufficient impact to be in a journal article.

Firstly, there was some concern that the fine dividing material in between the resolvable grain pattern in the film was some residual organic material leftover from the sacrificial support, in some complexing state with the metal surfaces making them insoluble in the thin film state. Organic materials are often problematic in any surface-based analytical instrumentation such as x-ray spectrophotometry (XPS) and secondary-ion mass spectrometry (SIMS). A common method for removing atmoshperic-borne organics, sometimes referred to as adventitious carbon, is to expose the surface to an oxygen plasma. An oxygen plasma cleaner is a common instrument in laboraties where such studies are routinely performed. At Pacific Northwest National Laboratory, there was opportunity to attempt a before-after test using the TEM there to look at a platinum film and look to see if the film survives such a test. In short, it did, and based on energy-dispersive spectroscopy, the carbon signal clearly goes down by a significant margin, though the metal signal remains the same (using the same spot size, and intensity is corrected for the different integration time). This data is shown in Figure A1.

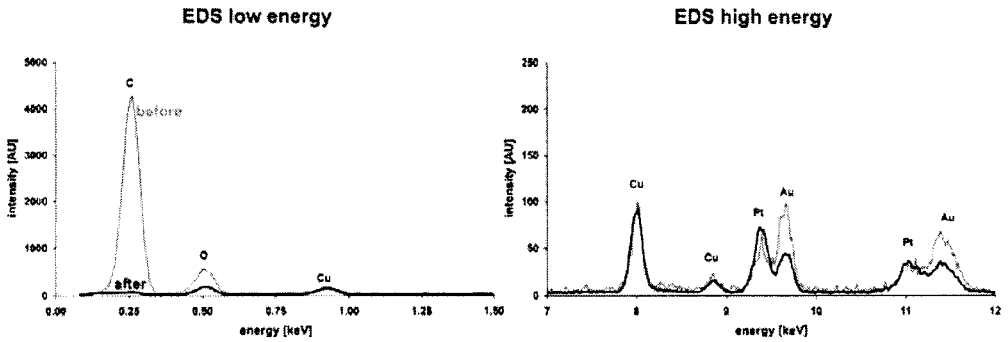

Figure A1: Energy-dispersive spectroscopy (EDS) of Pt films before (black) and after (gray) oxygen-plasma treatment. Note the precipitous drop in carbon content in the film, and that the platinum itself remains.

Figure A1 shows a couple of things. First, note the number of elements shown, carbon and oxygen (both contaminants), copper and gold (both from fluorescence), and platinum (the substrate). Electron energy-loss spectroscopy would be better but it was not set up at the time. The fluorescence issue explains the copper and gold, they come from the proximity of the probe (the electron beam) to the sample holder (brass) and especially, the grid itself (gold). The variation in the gold signal is likely attributed to the fact that the proximity of the beam to the edge of a grid window is a large contribution to the fluorescence signal there and the "after" spectrum is not of the identical position, only of the same spot size. However, copper fluorescence comes from the holder most likely, so it matters not the precise beam placement. The finding of significance here is that the platinum film is still intact up to 200 kV accelerating voltage after 15 minutes in an oxygen-plasma cleaner, and that the carbon signal has dropped significantly, even though the cleaned metal film was exposed to the atmosphere again for about five minutes while waiting to get back in the microscope due to other users. The carbon signal is even *less* than copper fluorescence. There is a possibility here for using EELS or EDS to do analytical chemical analyses on carbon-containing compounds with such a low background of this element on a support film that is not made of this material.

Additional applications of these films would involve any situation where one would want to look at a *surface* and where more information is sought than can be obtained by scanning probe microscopy or scanning electron microscopy (because those methods are already possible and generally easier to perform). Essentially, the *surface* itself is tantamount to preparing a sample, it not merely a support, it is integral. Because noble metal films were already made, the first efforts were directed towards functionalizing them with alkylthiols, molecules which make chemical bonds to metal surfaces via metal-sulfur bonds. In general, only noble metals will present such a surface, base metals will presence an oxide surface, and silica and carbon are not candidates. These functionalized surfaces are nearly always visualized by scanning probe microscopy, though scanning electron microscopy can also see them if patterns are made. It is believed that Figure A2 is the first demonstration that patterned surfaces containing alkanethiols can be seen in TEM.

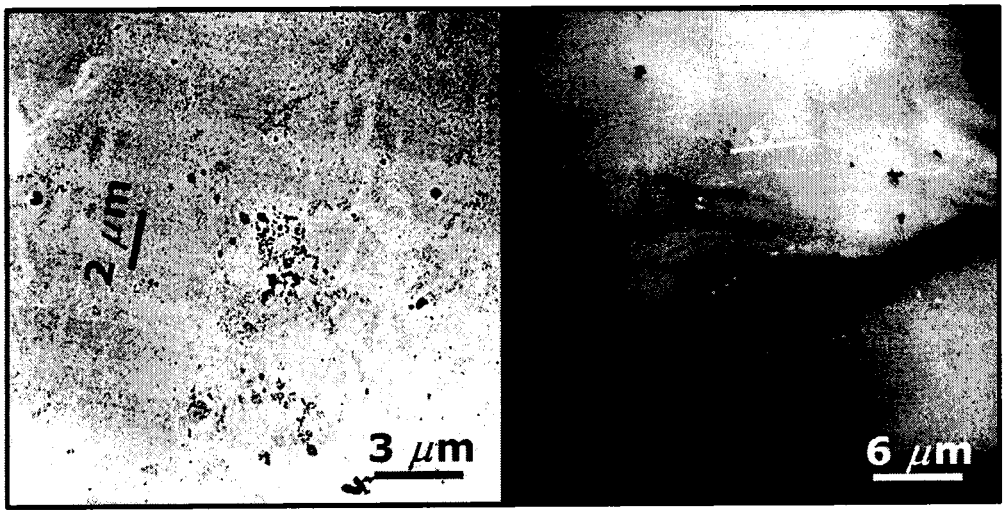

Figure A2: TEM images of octadecanethiol microcontact printed onto AuPd films, then loaded onto gold TEM grids and imaged. The brighter regions are the thiol-coated regions, based on the right image which was made from a non-symmetric stamp.

Although the contrast is very poor, in fact, the darker regions are actually the bare surface regions (G. M. Whitesides previously concluded that the coating passivates

those regions from contaminant adsorption, thus contrast appears as a result, in the SEM studies), and the darkness results from the slight amount of adventitious carbon that accumulates there over time before imaging. One approach to make this more useful as a TEM sample would be to use terminal groups that are used to crystallize materials out of some solution, like biomineralization, or anything else where TEM dominates over other techniques and where sample preparation should be avoided.

In another patterning approach, electron-beam lithography was toyed with to make scattering masks; as the films are transparent it was considered a potential candidate for electron projection lithography. Figure A3 shows two examples of some cobalt patterns made by electron-beam lithography as seen in TEM.

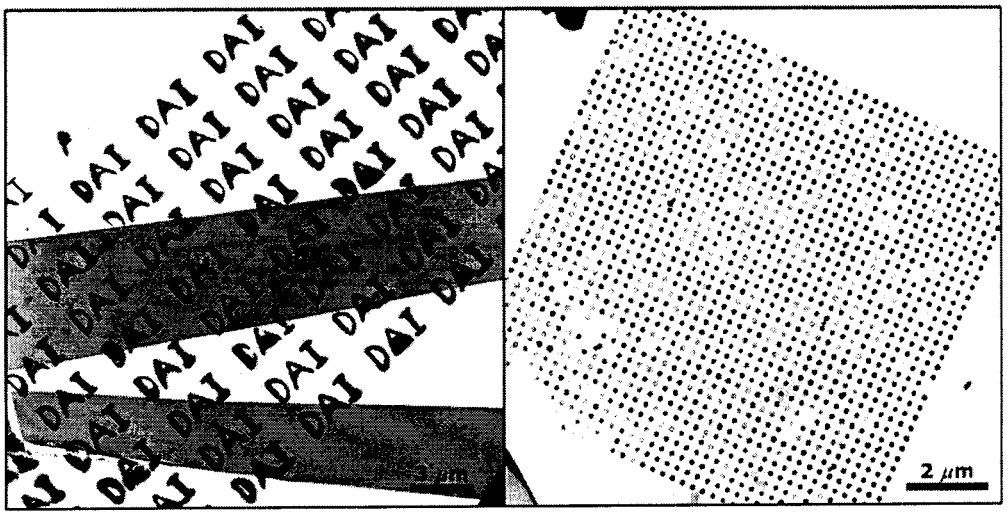

Figure A3: Electron-beam lithography using JC Nabity Lithography System software on a JEOL-7000 SEM, with 200-nm PMMA resist (no baking) spin-cast onto a Pt-film which was tacked down onto a small piece of Si using the sugar-aerosol solution as noted in Chapter 2. After spin-coating, the grid was extracted by adding water, then patterned in the SEM, developed, cobalt pulse plated at -1100 mV vs. SCE 6 times for 0.5 seconds ON and at open circuit for 1.5 seconds OFF, then the resist was removed with acetone. The film was made using the earlier ink technique mentioned in Chapter 2, hence the folds in the left figure (bands of darkness).

For those curious, the letters "DAI" correspond to the last name of a previous colleague who was learning lithography at the time. Note the dark band patterns.

This is due to the folding of the metal film because the film was made using the older method of picking up the film after stripping it from a sacrificial support. These flattened wrinkles appear from place to place to allow for drainage of fluid during drying. These regions are triple the original thickness, so if the film itself is 2 nm, then the dark bands are 6 nm thick, thus thin films for heavy metals are absolutely essential to maintain good image quality, every nanometer counts.

Lastly, films of iron were electrodeposited onto Pt to try building carbon nanofibers, ultimately to test the idea of patterning them using the S-layers. This work was performed by collaboration with Alan Cassell at NASA-AMES, CA. The SEM and TEM data are shown in Figure A4.

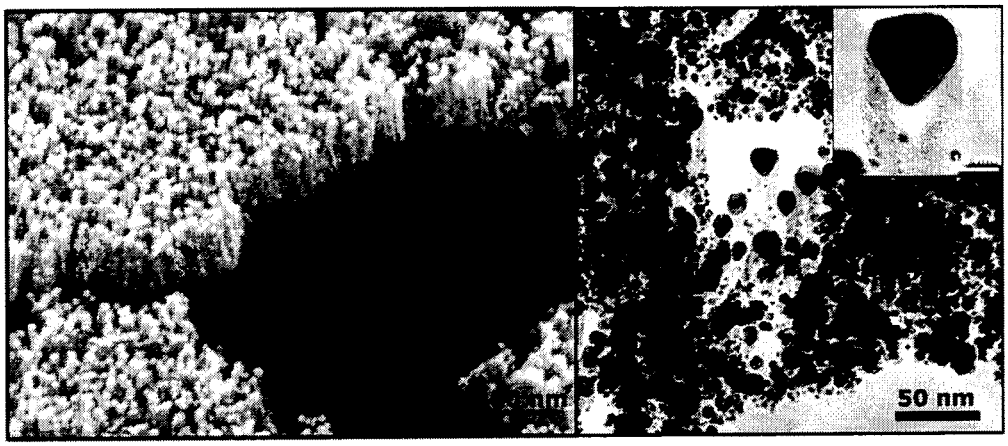

Figure A4: SEM (left) and TEM (right) of carbon nanofibers (CNFs) grown on iron-plated Pt coated grids by plasma-enhanced chemical vapor deposition (PE-CVD) by Dr. Alan Cassell at NASA-AMES.

It is interesting to note that on regular bulk substrates, often times a barrier layer is used to separate the catalyst particle film from the substrate. There is some speculation that during plasma bombardment, the local surface temperature may reach a point where the catalyst particle may alloy with this barrier layer and some attempt has been made to analyze the bed layer to see if any homogenization has occurred. Unfortunately, after cross-sectioning and ion-milling, one can not discern whether homogenization has occurred because of ion bombardment or ion milling. Of course, the sample shown here has not been subjected to any such preparation.

VITA

Daniel B. Allred Jr. was born in Austin, Texas in 1974 but constantly moved throughout childhood, being the son of a member of the armed forces. He enrolled in the University of Washington in 1992 with the intent of majoring in Business. He started a small business in 1993 and stopped it in 1994. He left college for some time and had other adventures. After returning in 1997 he majored in Chemical Engineering, for which he obtained his Bachelor's Degree in 2000. He then interned at Pacific Northwest National Laboratory for a summer to work on reformers in fuel cell microreactors and then worked in the Physics department at this University on a CERN project to build particle detectors for the Large Hadron Collider on the border of France and Switzerland. After learning of an opportunity to get into graduate school at this University he decided to turn down a chance at a staff position and instead entered the Graduate School in this University in 2001.